© 2022. Published by The Company of Biologists Ltd | Development (2022) 149, dev200515. doi:10.1242/dev.200515

RESEARCH ARTICLE

Alignment of the cell long axis by unidirectional tension acts cooperatively with Wnt signalling to establish planar cell polarity

Sayuki Hirano[1], Yusuke Mii[2,3,4,5], Guillaume Charras[6,7,8] and Tatsuo Michiue[1,*]

ABSTRACT

Planar cell polarity (PCP) is the aligned cell polarity within a tissue plane. Mechanical signals are known to act as a global cue for PCP, yet their exact role is still unclear. In this study, we focused on PCP in the posterior neuroectoderm of *Xenopus laevis* and investigated how mechanical signals regulate polarity. We reveal that the neuroectoderm is under a greater tension in the anterior-posterior direction and that perturbation of this tension causes PCP disappearance. We show that application of uniaxial stretch to explant tissues can control the orientation of PCP and that cells sense the tissue stretch indirectly through a change in their shape, rather than directly through detection of anisotropic tension. Furthermore, we reveal that PCP is most strongly established when the orientation of tissue stretch coincides with that of diffusion of locally expressed Wnt ligands, suggesting a cooperative relationship between these two PCP regulators.

KEY WORDS: Mechanical signal, Tension, Planar cell polarity (PCP), Neuroectoderm, Wnt

INTRODUCTION

Planar cell polarity (PCP) is the aligned cell polarity established within the plane of a cell sheet and is an essential property that allows the accurate development of animal tissues (Butler and Wallingford, 2017). PCP is regulated by evolutionarily conserved core PCP components, including transmembrane proteins Flamingo (Celsr in vertebrates), Van Gogh (Vangl) and Frizzled (Fzd) together with cytoplasmic proteins Prickle and Dishevelled (Dvl) (Butler and Wallingford, 2017; Devenport, 2014; Gray et al., 2011; Singh and Mlodzik, 2012). These localize to apicolateral junctions and form two kinds of stable complexes, Flamingo/Vangl/Prickle and Flamingo/Fzd/Dvl, which show mutually exclusive localization within cells, thereby establishing an axis of polarisation (Devenport, 2014; Peng and Axelrod, 2012). PCP is observed in many tissues, and defects in core PCP components cause various developmental disorders (Goodrich and Strutt, 2011; Jenny, 2010; Singh and Mlodzik, 2012; Wang and Nathans, 2007).

Although the molecular mechanisms that organise PCP components within a cell and across intercellular junctions have been well investigated (Axelrod, 2013; Chen et al., 2008; Tree et al., 2002; Wu and Mlodzik, 2008), the long-range determinants that establish the initial axis of cell polarity within the tissue remain controversial and several candidates have been proposed, including biochemical gradients and mechanical cues. One well-studied candidate is a tissue-wide gradient of Wnt ligands (Gao et al., 2011; Qian et al., 2007; Sokol, 2015). Indeed, some ectopically expressed Wnt ligands can alter the polarity of the surrounding cells (Chu and Sokol, 2016; Wu et al., 2013), indicating a role in instructing planar polarity. However, in the *Drosophila* wing, which is the most popular model for PCP studies, loss-of-function experiments targeting Wnt genes do not cause PCP defects (Ewen-Campen et al., 2020; Yu et al., 2020), suggesting that there is redundancy in the global cues instructing PCP. Another candidate cue is mechanical signalling. It has been shown that actomyosin activity and the forces it generates contribute to PCP formation (Luxenburg et al., 2015; Mahaffey et al., 2013; Ossipova et al., 2015), and it has been proposed that mechanical stimuli derived from morphogenetic movements regulate the direction of polarity through the realignment of microtubules (Chien et al., 2015) or the rearrangement of cells or junctions (Aigouy et al., 2010; Aw et al., 2016; Butler and Wallingford, 2018). However, the exact role of mechanical forces in PCP remains unclear due to the difficulty of characterising and manipulating these forces. To investigate the mechanism by which mechanical forces regulate PCP, we focused on PCP in the posterior neuroectoderm of *Xenopus laevis* and the morphogenetic movements that occur alongside its establishment.

PCP in the posterior neuroectoderm of *Xenopus* arises during late gastrula and early neurula stages. Polarity is established along the anterior-posterior (AP) axis, and anterior localization of the Vangl/Prickle complexes can be observed by stages 12.5-13 (Ossipova et al., 2015). During the whole PCP establishment stage, neuroectodermal tissue is subjected to a unidirectional stretch along the AP axis arising from morphogenetic movements such as gastrulation and body elongation. Thus, we hypothesized that mechanical tension or tissue deformation may act as global cues to instruct cell polarity and we examined their roles by applying chemical and mechanical perturbations to the tissue. We show that application of uniaxial stretch to explant tissues can control the orientation of PCP and that cells sense the tissue stretch indirectly through a change in their shape rather than directly through detection of anisotropic tension. Furthermore, we reveal that PCP is most strongly established when the orientation of tissue stretch coincides with that of diffusion of locally expressed Wnt ligands, suggesting a cooperative relationship between these two PCP regulators.

[1]Department of Life Sciences (Biology), Graduate School of Arts and Sciences, The University of Tokyo, 3-8-1 Komaba, Meguro, Tokyo 153-8902, Japan. [2]National Institute for Basic Biology and Exploratory Research Center on Life and Living Systems, National Institutes of Natural Sciences, 5-1 Higashiyama, Myodaiji-cho, Okazaki 444-8787, Japan. [3]Exploratory Research Center on Life and Living Systems, National Institutes of Natural Sciences, 5-1 Higashiyama, Myodaiji-cho, Okazaki 444-8787, Japan. [4]Department of Basic Biology, Graduate School for Advanced Studies (SOKENDAI), 5-1 Higashiyama, Myodaiji-cho, Okazaki 444-8787, Japan. [5]Japan Science and Technology Agency, PRESTO, 4-1-8 Honcho, Kawaguchi, Saitama 332-0012, Japan. [6]London Centre for Nanotechnology, University College London, 17-19 Gordon Street, London WC1H 0AH, UK. [7]Department of Cell and Developmental Biology, University College London, Gower Street, London WC1E 6BT, UK. [8]Institute for the Physics of Living Systems, University College London, Gower Street, London WC1E 6BT, UK.

*Author for correspondence (tmichiue@bio.c.u-tokyo.ac.jp)

S.H., 0000-0001-7183-6604; T.M., 0000-0001-9047-0513

Handling Editor: Thomas Lecuit
Received 11 January 2022; Accepted 6 May 2022

Development (2022) 149, dev200515. doi:10.1242/dev.200515

RESULTS

Establishment of PCP in the anterior-posterior direction begins when cells elongate along the AP axis

We first characterised the time course of establishment of PCP on the posterior neuroectoderm of *Xenopus laevis*. Embryos at stages 12 to 14 were immunostained for Vangl2 and ZO-1 as markers of planar polarity and cell shape, respectively. Vangl2 showed an anterior localization from around stage 13 (Fig. 1A), consistent with previous work (Ossipova et al., 2015). At stage 12.5, the expression level of Vangl2 was low, and a slight anterior localization was observed in some cells. At stage 13, many cells showed anterior Vangl2 polarization, which was maintained at stage 14. We quantified Vangl2 polarization using the method published in a previous study (Strutt et al., 2016) and confirmed that the polarity axis showed clear AP orientation at stage 13 and 14 (Fig. 1B). We also characterised cell shape change based on ZO-1 images and found that cells were elongated in the AP direction at stages 12.5 to 13, when the AP planar polarity first appeared (Fig. 1A, lower panels). The neuroectoderm at these stages is thought to be subjected to tension along the AP axis due to morphogenetic movements such as gastrulation and body elongation, and we hypothesized that this unidirectional tension may act as a global cue to direct planar polarity.

Tension along the AP axis is necessary for the establishment of PCP

During the PCP establishment stage, neuroectodermal cells become elongated in the AP direction, probably due to morphogenetic movements. We examined whether the neuroectoderm is indeed subjected to anisotropic tension by observing tissue recoil in laser ablation experiments. A small region of the posterior neuroectoderm (three to five cells in width) was cut at stage 12, and the width of the resulting wound was measured immediately after cutting as a proxy for tissue tension. We first verified that the cutting affected only the outermost layer of the neuroectoderm (Fig. S1A). Laser cutting was performed in two orientations, perpendicular or parallel to the AP body axis (Fig. 2A,B), and in two locations, close (five to ten cell diameters away) to the blastopore or far (15-20 cell diameters away) from it. For both locations, the wound was larger when tissue was cut perpendicularly to the AP body axis rather than parallel to it (Fig. 2C), indicating that the posterior neuroectoderm is under greater tension in the AP direction. When tissue was cut perpendicularly to the AP axis, the cellular aspect ratio significantly decreased on the anterior and posterior sides of the cut, while the aspect ratio of the cells on the left and right sides of the cut did not change significantly when the tissue was cut parallel to the AP axis (Fig. S1B-D). These results indicate that the endogenous tension along the AP axis was indeed relaxed by the cut that was perpendicular to the AP axis.

We next examined whether tension is necessary for PCP formation. Embryos were injected with mRNAs encoding mRuby2-Prickle3 and membrane-tethered GFP as markers of planar polarity and cell shape, respectively. Prickle is one of the core PCP proteins, known to interact directly with Vangl and to be polarized towards the anterior side of cells (Butler and Wallingford, 2017; Ossipova et al., 2015). An appropriate amount of mRNA encoding Vangl2 was also injected because exogenous Prickle or Vangl2 do not polarize when only one of them is overexpressed (Jenny et al., 2003; Ossipova et al., 2015). A small region of the neuroectoderm was cut at stage 12, immediately before the emergence of AP planar polarity, and the embryos were incubated until stage 14, when clear AP planar polarity is observed in wild-type embryos. Mesodermal convergent extension is the primary determinant of axis elongation (Wallingford and Harland, 2001), and thus our cutting procedure does not affect body elongation itself. The wounds did not heal between stages 12 and 14, signifying that the cuts provide a long-lasting dissipation of tissue tension. When cuts were performed perpendicularly to the AP body axis, the anterior localization of mRuby2-Prickle3 almost disappeared (Fig. 2D,E) in the region where the tension was relaxed

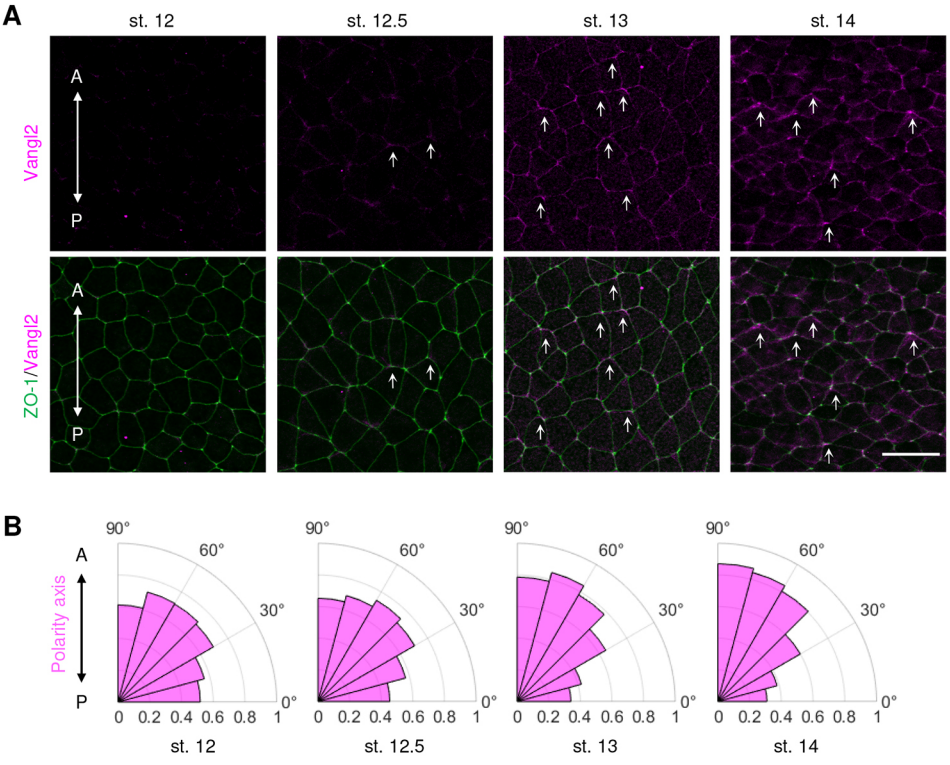

Fig. 1. Establishment of PCP in the anterior-posterior direction begins when cells elongate along the AP axis. (A) Fluorescence images of the posterior neuroectoderm from stage 12 to 14. Arrows indicate the accumulation of Vangl2 at the anterior side of the cell. Scale bar: 50 µm. (B) Plots of the polarity axis calculated from Vangl2 localization. The area of each bin represents the relative number of observations. *n*=5 (stage 12), 6 (stage 12.5), 7 (stage 13) and 6 (stage 14) embryos. The data were obtained from five independent experiments. A, anterior; P, posterior.

Development (2022) 149, dev200515. doi:10.1242/dev.200515

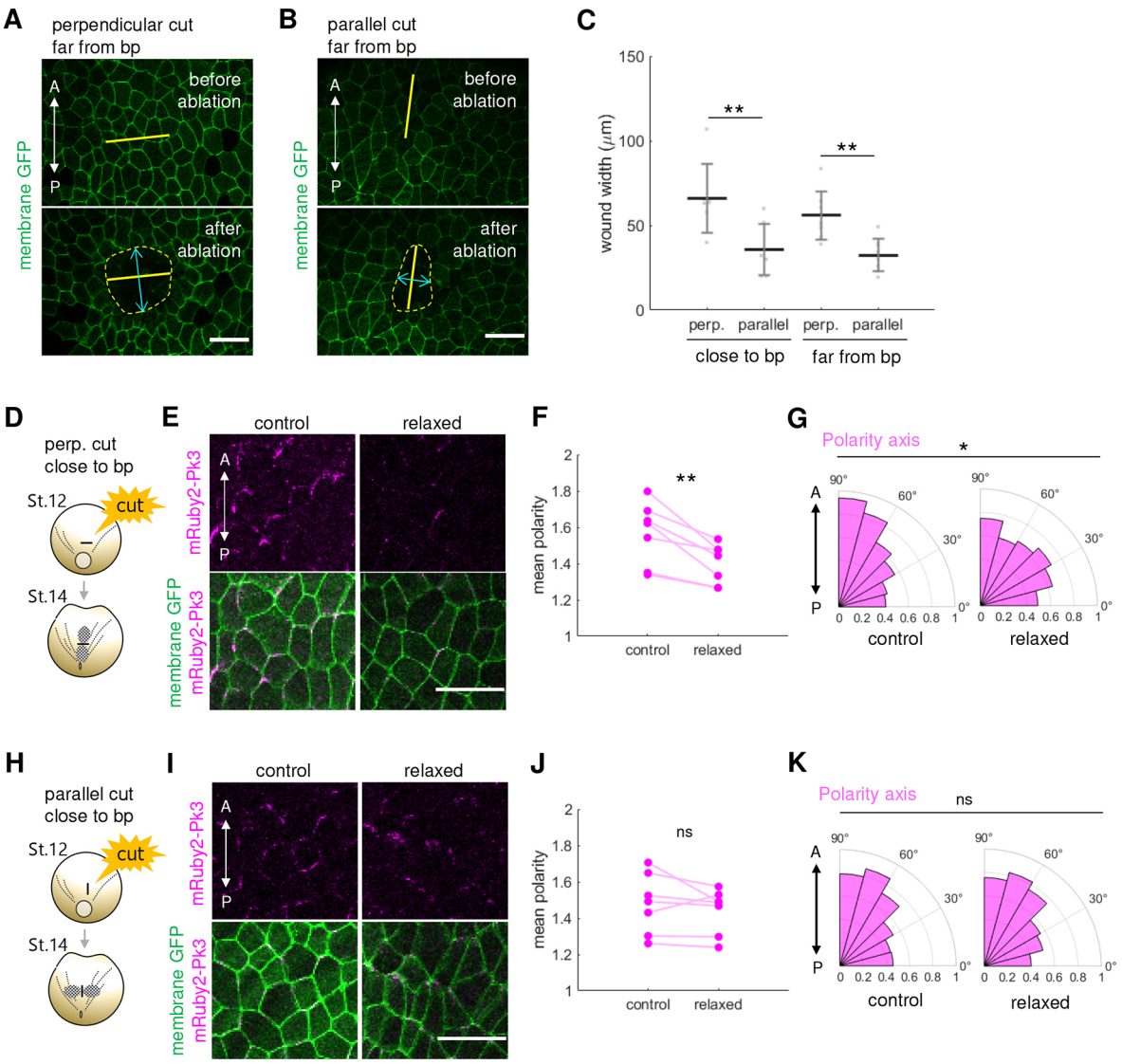

Fig. 2. Tension along the AP axis is necessary for the establishment of PCP. (A,B) Fluorescence images of the embryos at stage 12 before and after laser cutting perpendicular (A) or parallel (B) to the AP body axis. Solid yellow lines indicate the cutting sites; dotted yellow lines indicate the wounds; solid cyan lines indicate the width of the wound perpendicular to the cutting line. Scale bars: 50 µm. (C) Plots of the wound width made by laser cutting. *n*=7 embryos for perpendicular cut close to the blastopore (bp), *n*=7 embryos for parallel cut close to bp, *n*=8 embryos for perpendicular cut far from bp and *n*=8 embryos for parallel cut far from bp. Data are mean±s.d. (D,H) Schematic images of laser ablation experiments. (E,I) Fluorescence images of control and relaxed areas in laser ablation experiments. The 'relaxed' image in E shows the anterior side of the cut. Scale bars: 50 µm. (F,J) Plots of the mean polarity. Lines connect data from the same embryo. (G,K) Plots of the polarity axis. The area of each bin represents the relative number of observations. *n*=7 embryos in E-G,I-K. The data were obtained from four independent experiments. A, anterior; P, posterior; bp, blastopore. Statistical significance was tested using a two-tailed Mann–Whitney *U*-test in C, a two-tailed Wilcoxon signed rank test in F,J, and a Kuiper test in G,K. **P*<0.05, ***P*<0.01. See also Figs S1, S2.

(grey area in Fig. 2D). We quantified Prickle3 polarization using the same method as mentioned above and examined changes in the mean polarity value. The mean polarity value is the indication of heterogeneity of the protein localization on the cell membrane: if the protein is concentrated in a specific region on a cell membrane, this value becomes larger, whereas if the protein is spread over a wide region, this value becomes smaller (see Materials and Methods). When the neuroectodermal tissue was cut perpendicularly to the AP axis, the mean polarity value significantly decreased in the relaxed area (Fig. 2F). The distribution of the polarity axis did not show any specific orientation in the relaxed area, while it was oriented in the AP direction in the control (Fig. 2G). This likely results from loss of membrane localization of mRuby2-Prickle3, rather than a change in the direction of polarity. Similar results were also obtained when the tissue was cut perpendicularly to the AP axis in a region further from the blastopore (Fig. S2A-D), but in this case the distribution of polarity axis still showed a bias towards AP. The mean polarity value decreased on both anterior and posterior sides of the cut (Fig. S2I,J), and did not significantly change in the region further from the cut (more than 10 cell diameters away from the cut) (Fig. S2K). Thus, the relaxation of tension and its effect on polarity formation depend on the distance from the cut. In contrast, when the tissue was cut in parallel to the AP axis, no significant change was observed in either the mean polarity or the polarity axis (Fig. 2H-K, Fig. S2E-H). These results indicate that the posterior neuroectoderm is subjected to a greater tension along the AP axis and that this tension is necessary for membrane localization of Prickle3 and the establishment of planar polarity.

Development (2022) 149, dev200515. doi:10.1242/dev.200515

The orientation of planar polarity is controlled by the direction of tissue stretch

We hypothesized that the orientation of planar polarity might be controlled by tissue tension. To examine this possibility, we developed a tissue-stretching system (Fig. 3A). Posterior neuroectodermal tissue was dissected from an embryo at stage 10.5 (early gastrula stage) and immediately placed in a chamber coated with fibronectin. These explants were then incubated until the sibling embryos reached stage 12, and a unidirectional stretch was applied gradually from stage 12 to 14. As a control, explants were incubated under the same conditions without stretch. Before stretch, mRuby2-Prickle3 did not display any preferential orientation (Fig. 3B). After stretch at stage 14, mRuby2-Prickle3 appeared strongly localized to specific regions of the membrane (Fig. 3B), and the mean polarity value increased compared with stage 12, although the difference was not significant (Fig. 3C). All the tissues at stage 14 showed similar mean polarity values, regardless of whether they were stretched or not. The direction of cellular major axis aligned with the direction of tissue stretch (Fig. 7D), as did the direction of mRuby2-Prickle3 accumulation (Fig. 3B,D). In the explants stretched in the AP direction, mRuby2-Prickle3 accumulated at the AP interfaces of cells and the polarity axis was biased toward AP. On the other hand, when the explants were stretched in medial-lateral (ML) direction, mRuby2-Prickle3 accumulated at the ML interfaces, and the polarity axis was biased toward ML. As the stretch changed cell shape significantly, we re-analysed the data in Fig. 3 using a different polarity quantification method based on principal component analysis (PCA) (Tan et al., 2021) to examine whether the results reflected the differences in cell shape. This analysis further confirmed our results (Fig. S3). The mean polarity values were similar for stretched and unstretched samples, and the polarity axis was oriented in the direction of tissue stretch. These results show that tissue stretch plays a significant role in determining the orientation of planar polarity.

The alignment of tissue stretch and Wnt diffusion allows clear PCP formation

Unidirectional tissue stretch changed the orientation of the polarity axis, but the extent of polarity alignment was not the same between AP-stretched and ML-stretched explants. The polarity axis was well aligned in the AP direction in the AP-stretched explants, while in the ML-stretched explants, it was not perfectly oriented in the ML direction, but rather showed a peak around 30-45° (Fig. 3D). We hypothesized that this difference might arise from Wnt signalling, which is thought to provide another global cue for PCP establishment. Wnt11 is known to be involved in the regulation of PCP in *Xenopus* ectoderm and is expressed in the posterior region of early gastrula (Carron et al., 2005; Ku and Melton, 1993). This

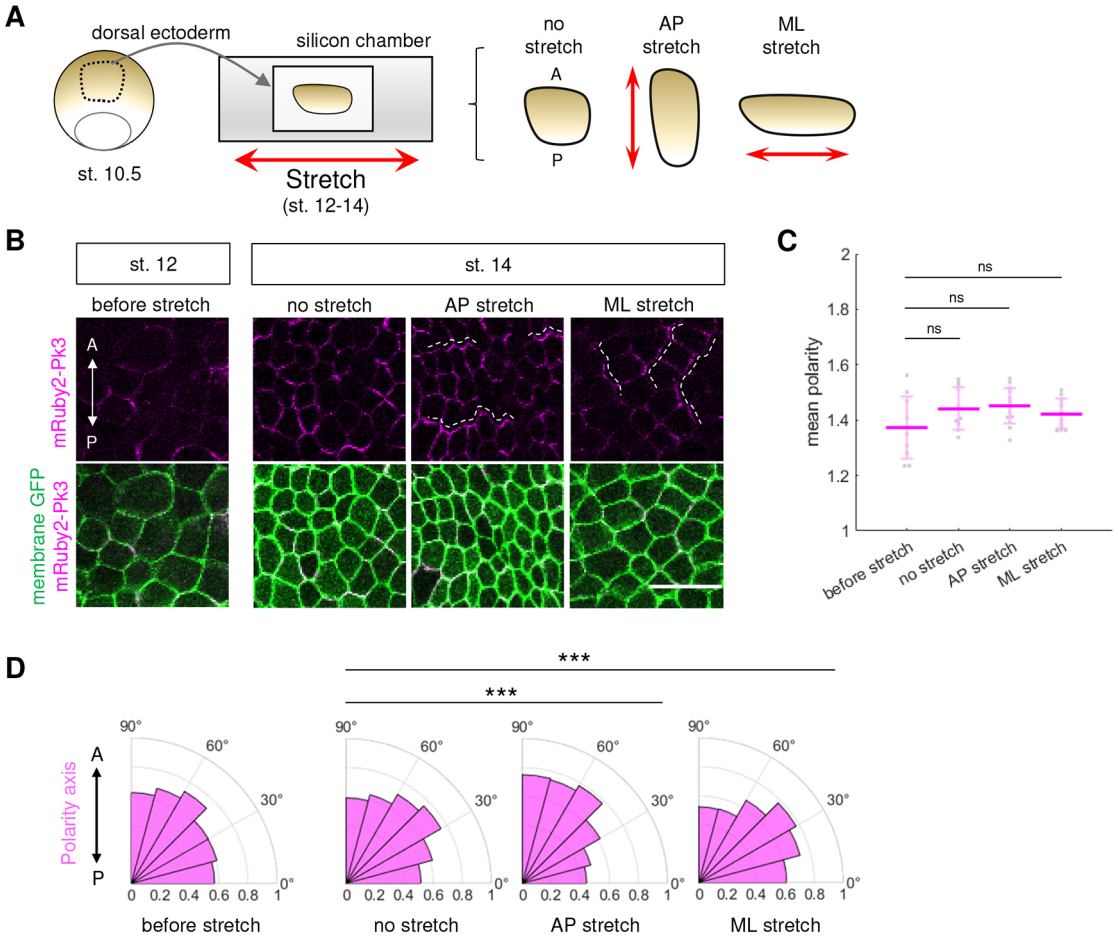

Fig. 3. Orientation of planar polarity is controlled by the direction of tissue stretch. (A) Schematic image of tissue-stretching experiments. (B) Fluorescence images of explants before and after stretch. Dotted lines indicate cell-cell interface where mRuby2-Prickle3 accumulated. Scale bar: 50 µm. (C) Plots of the mean polarity. Data are mean±s.d. (D) Plots of the polarity axis. The area of each bin represents the relative number of observations. *n*=10 (before stretch), *n*=11 (no stretch), *n*=15 (AP stretch) and *n*=12 (ML stretch) explants. The data were obtained from three independent experiments. Statistical significance was tested using a two-tailed Mann–Whitney *U*-test in C and a Kuiper test in D. ***P<0.001. See also Fig. S3.

Development (2022) 149, dev200515. doi:10.1242/dev.200515

localised expression of Wnt ligand is assumed to create a Wnt signalling gradient, which has been proposed to regulate the direction of PCP (Gao et al., 2011; Wu et al., 2013). Consistent with this, ectopically expressed Wnt11 can alter the polarity of surrounding cells (Chu and Sokol, 2016), indicating an ability to instruct polarity. In our explant stretching experiments, the posterior neuroectoderm was dissected at stage 10.5, when localised expression of Wnt11 is already observed. We hypothesized that cell polarity was better aligned when the direction of tissue stretch coincided with that of diffusion of this locally expressed Wnt11 (AP-stretched explants) than when they were perpendicular to one another (ML-stretched explants). To test this, we examined (1) whether the difference between AP-stretched and ML-stretched explants could be eliminated by inhibiting the endogenous Wnt signalling and (2) whether the polarity axis would be better aligned with ML stretch when Wnt11 was ectopically expressed to form the direction of its diffusion in the ML direction.

First, we inhibited endogenous Wnt signalling by overexpressing the secretory protein Crescent. Crescent interacts with Wnt11 and inhibits non-canonical Wnt signalling in the neuroectoderm (Shibata et al., 2005). When *Crescent* mRNA was injected into an eight-cell embryo with 50 pg per blastomere, the membrane localization of mRuby2-Prickle3 disappeared almost completely, making it difficult to quantify polarity (Fig. S4A, right). When we injected half this amount of *Crescent* mRNA, PCP formation was partially inhibited (Fig. S4A, middle). Some cells still showed anterior polarization of mRuby2-Prickle3, but its membrane localization was more sparse than in the control embryos. As

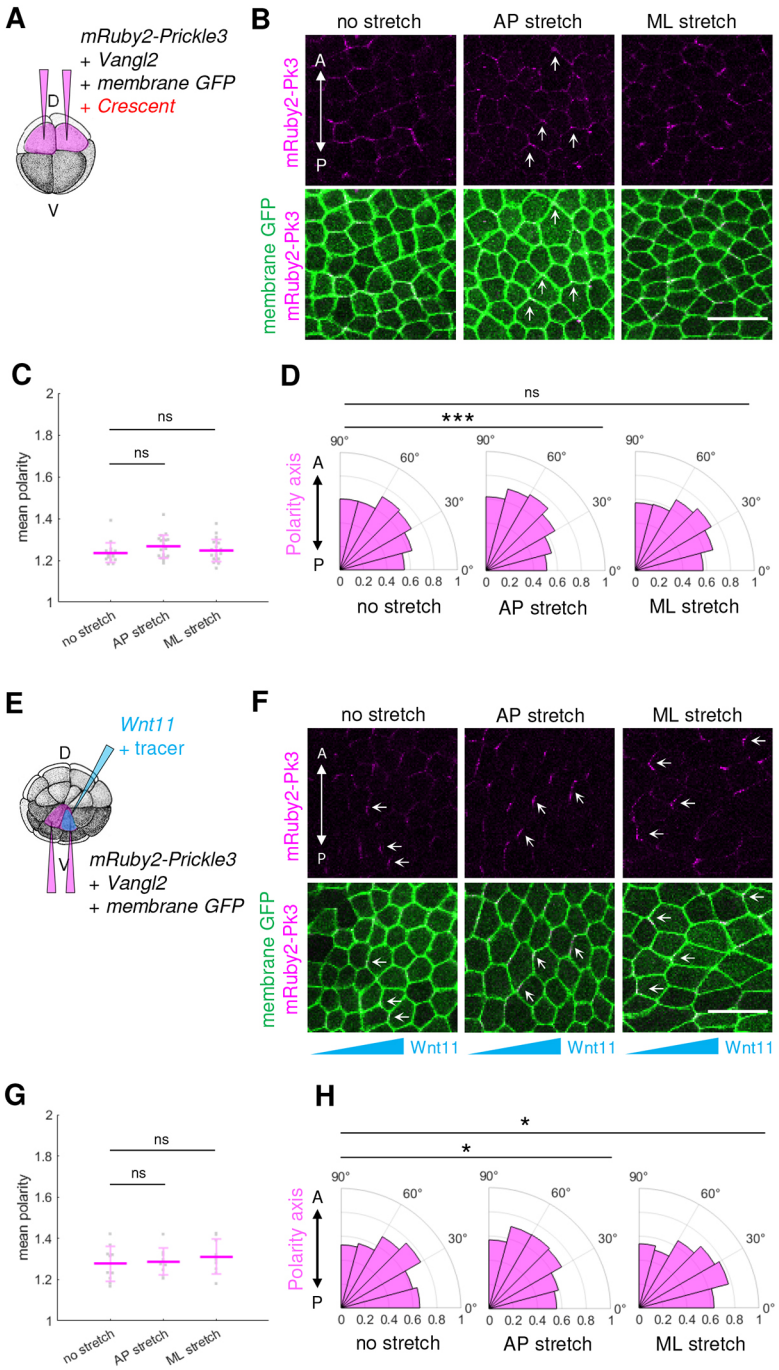

Fig. 4. The alignment of tissue stretch and Wnt diffusion allows clear PCP formation. (A,E) Schematic images of mRNA injection. D, dorsal; V, ventral. (B,F) Fluorescence images of explants. Arrows indicate the accumulation of mRuby2-Prickle3. Wnt ligand source is on the right side of the images in F. Scale bar: 50 µm. (C,G) Plots of the mean polarity. Data are mean±s.d. (D,H) Plots of the polarity axis. The area of each bin represents the relative number of observations. *n*=18 (no stretch), *n*=20 (AP stretch) and *n*=20 (ML stretch) explants in B-D; *n*=10 (no stretch), *n*=9 (AP stretch) and *n*=9 (ML stretch) explants in F-H. The data were obtained from four (B-D) or three (F-H) independent experiments. Statistical significance was tested using a two-tailed Mann–Whitney *U*-test in C,G and using a Kuiper test in D,H. **P*<0.05, ****P*<0.001. See also Fig. S4.

Development (2022) 149, dev200515. doi:10.1242/dev.200515

quantification of polarity was possible, we carried out explant stretching experiments in this condition. Without stretch, mRuby2-Prickle3 did not show any polarization, as expected if both the Wnt and the mechanical cues are absent (Fig. 4A,B). By stretching in the AP direction, some cells showed anterior localization of mRuby2-Prickle3 and the distribution of the polarity axis was biased towards the AP direction compared with unstretched explants (Fig. 4B,D). Importantly, the polarity axis was less aligned when Wnt signalling was perturbed than in control AP-stretched explants (Figs 3D and 4D). In ML-stretched explants, no clear polarity direction emerged (Fig. 4D). Regarding the mean polarity, there was no significant difference between stretched and unstretched explants, as was the case without Crescent overexpression (Fig. 4C). Based on these results, we hypothesized that unidirectional tissue stretch is a regulator of the polarity axis that acts together with the Wnt signalling. The inhibition of Wnt signalling by Crescent overexpression was only partial (Fig. S4A), and therefore stretch might cooperate with the remnant of the Wnt signalling to continue to induce AP polarization in the AP-stretched explants. As no clear polarity alignment was observed in the ML-stretched explants, tissue stretch alone might not be sufficient to induce PCP. Alternatively, the magnitude of deformation applied in our experiments might not be sufficient, and a larger stretch might be able to induce PCP alone.

Next, we ectopically expressed Wnt11 to direct its diffusion in the ML direction. In this experiment, ventral ectodermal tissue was used to reduce the effect of endogenous Wnt11, which is more strongly expressed in the dorsal region (Ku and Melton, 1993; Shibata et al., 2005). *Wnt11* mRNA was injected into one side of the embryo at the 32-cell stage (Fig. 4E), and ventral ectoderm was dissected and stretched as in Fig. 3. Without stretch, the accumulation of mRuby2-Prickle3 was already biased towards the ML-interface of the cells (Fig. 4F), consistent with previous work (Chu and Sokol, 2016). When the explants were stretched in the ML direction, the biased localization of mRuby2-Prickle3 became clearer and the distribution of the polarity axis was more aligned in the ML direction (Fig. 4F,H). In AP-stretched explants, the polarity axis was reoriented towards the AP direction compared with unstretched explants (Fig. 4H). However, the orientation of polarity was not perfectly aligned with the AP direction but showed an intermediate orientation between the direction of tissue stretch and that of Wnt diffusion (Fig. 4F,H). Similar results were obtained when the amount of *Wnt11* mRNA was doubled, indicating that simply increasing the amount of Wnt ligand is not capable of overriding the effect of tissue stretch (Fig. S4B,C). As for the mean polarity, again it did not display any significant difference between stretched and unstretched explants (Fig. 4G). These results suggest that tissue stretch is a regulator of the polarity axis that acts in addition to the Wnt signalling, and that clear PCP is established when both PCP regulators align in the same direction.

Cells do not detect tension as a cue for PCP

The results achieved so far indicate that tissue stretch plays a significant role in determining the polarity axis. However, it remains unclear what cue cells detect to determine the polarity axis when the tissue is stretched. One possibility is that cells directly detect tension or, alternatively, they may sense it indirectly by detecting tension-induced changes in cell shape or cytoskeleton orientation. In the following sections, we will examine each of these possibilities.

First, we examined whether cells directly detect tension. In our wounding experiments, we noticed that the width of the gap was larger for the cuts closer to the blastopore when we ablated the tissue perpendicularly to the AP body axis (Fig. 2C). This result suggests the presence of a gradient in tension along the AP axis that may act as a global cue to establish PCP. We confirmed the presence of a spatial gradient in tension by acquiring spatial maps of the apparent elasticity along the AP axis of the dorsal neuroectoderm at each developmental stage using atomic force microscopy (AFM) (Fig. 5A). The apparent elasticity is sensitive to the surface tension of cells, as well as to the elasticity of their cytoskeleton. In wild-type embryos, apparent elasticity increased dramatically with developmental stage, progressively rising from 50 Pa at stage 10, when PCP is not established, to over 300 Pa at stages 13 and 14, when PCP is established (Fig. 5B). Furthermore, moderate spatial gradients of apparent elasticity could be observed from posterior to anterior from stage 11 to 14, with slopes increasing from 0.09 Pa/µm to 0.21 Pa/µm (Fig. 5B), which is small compared with the gradients detected by tissue cultured cells (14 Pa/µm; Sunyer et al., 2016). When we imaged the organisation of F-actin and microtubules by immunostaining, we could not find a spatial gradient along the AP axis (Fig. S5A-D). This result suggests that a difference in actin and microtubule organization does not contribute to the gradient in apparent elasticity and that this gradient is due to a gradient in tension. We considered several possible mechanisms by which this gradient might regulate the direction of cell polarity. One possibility is that there is a threshold in tension required for the membrane localization of Prickle3 or other core PCP proteins, and that polarity is progressively established from the posterior side as the tension to which cells are subjected increases above threshold. The other possibility is that cells sense a gradient in tension across their length to establish their anterior and posterior sides, but that the absolute value of the tension is not important.

We examined whether polarity formation is controlled by the presence of a threshold of apparent elasticity. If this was the case, we would expect that PCP can only be established for apparent elasticities above ∼300 Pa based on our measurements at stages 13-14 (Fig. 5B). To decrease apparent elasticity, embryos were treated with blebbistatin, a myosin activity inhibitor, from stage 12 to 14, and apparent elasticity was measured at stage 14. Blebbistatin treatment decreased apparent elasticity across the entire measurement area compared with DMSO-treated embryos with values ranging from 250 Pa near the blastopore to 125 Pa further away from it (Fig. 5C). Despite the overall decrease in apparent elasticity, a gradient in apparent elasticity with a slope comparable with untreated samples was still observable. When we examined polarity at stage 14, we found that the blebbistatin-treated embryos showed a comparable polarity to the DMSO-treated embryos (Fig. 5D), with no significant change in either the polarity value or the polarity axis (Fig. 5E,F). These results show that PCP is established normally even when apparent elasticity is decreased to levels normally observed at developmental stages during which PCP does not occur. Thus, it is suggested that cells are not sensitive to the absolute value of tension when establishing PCP.

We next examined the possibility that cells are sensitive to a gradient in tension across their length to establish their anterior and posterior sides. Our experiments indicated that explants can robustly establish PCP when stretched (Fig. 3); therefore, if a gradient in tension was necessary for PCP, it should be present across stretched explants. To examine this, we mapped the apparent elasticity of the explants subjected to the same stretching procedures as previously described, before and after stretch along a 400 µm band in the centre of the explant along the stretch direction (Fig. 5G). For unstretched explants, measurements were conducted in a direction corresponding to the AP axis prior to dissection. At both stage 12

Development (2022) 149, dev200515. doi:10.1242/dev.200515

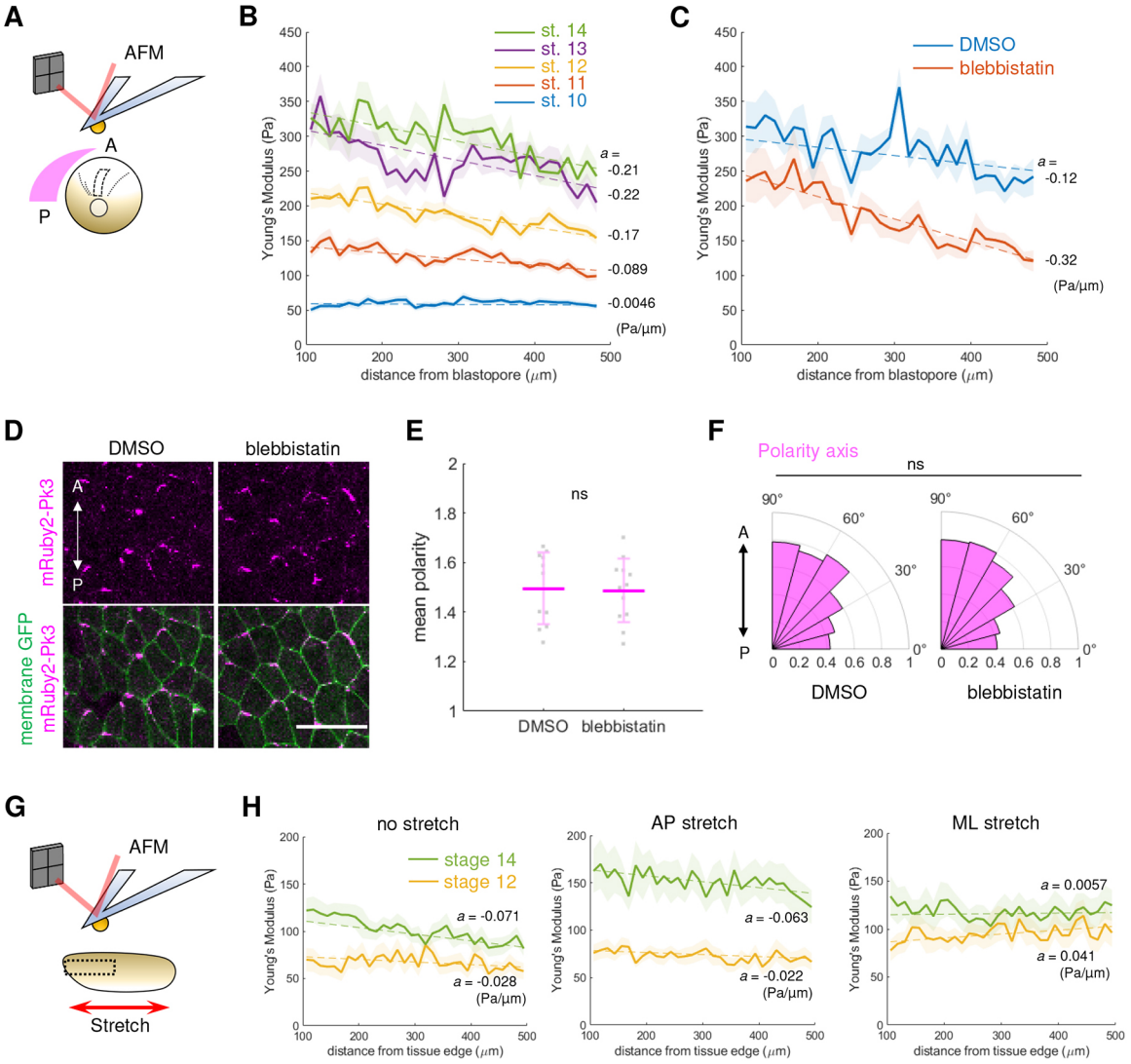

Fig. 5. Cells do not detect tension as a cue for PCP. (A) Schematic image of elasticity measurement for an embryo. (B) Plots of Young's modulus for stages 10 to 14. Data are mean±s.e.m. Dashed lines indicate the approximated lines by the least-squares method. The value *a* is the slope of the approximated lines. *n*=9 embryos for all stages. (C) Plots of Young's modulus of embryos treated with DMSO or 100 µM blebbistatin. Data are mean±s.e.m. Dashed lines indicate the approximated lines by the least-squares method. The value *a* is the slope of the approximated line. *n*=8 (DMSO) and *n*=7 (blebbistatin) embryos. (D) Fluorescence images of embryos treated with DMSO or 100 µM blebbistatin. Scale bar: 50 µm. *n*=11 (DMSO) and *n*=12 (blebbistatin) embryos in D-F. (E) Plots of the mean polarity. Data are mean±s.d. (F) Plots of the polarity axis. The area of each bin represents the relative number of observations. (G) Schematic image of elasticity measurement for explants. (H) Plots of Young's modulus for explants before and after stretch. Data are mean±s.e.m. Dashed lines indicate the approximated lines by the least-squares method. The value *a* is the slope of the approximated line. *n*=7 explants for all conditions. The data were obtained from 6 (B), 3 (C), 3 (D-F) or 5 (H) independent experiments. Statistical significance was tested using a two-tailed Mann–Whitney *U*-test in E and a Kuiper test in F. See also Fig. S5.

(before stretching) and stage 14 (after stretching), the apparent elasticity was lower than in embryos (Fig. 5B,H), perhaps because there is no contribution from tension arising in surrounding tissues and further confirming that the absolute value of tension is not important to establish PCP. After stretching, the apparent elasticity increased in all conditions, and this increase was most pronounced in AP-stretched explants (Fig. 5H). However, no clear gradient of apparent elasticity was observed in either the stretched or unstretched explants. Despite the lack of a gradient in apparent elasticity, polarity was established along the stretching direction.

These results indicate that cells do not directly sense tension as a cue for PCP; thus, we next examined whether the tension-induced changes in cytoskeleton orientation or cell shape play a significant role in determining the polarity axis.

The determination of the polarity axis by tissue stretch is not microtubule-mediated

Patterned alignments of microtubules have been observed in some planar-polarized tissues (Hannus et al., 2002; Shindo et al., 2008; Vladar et al., 2012) and it has been hypothesised that this induces biased vesicle trafficking that can lead to PCP establishment (Butler and Wallingford, 2017; Matis et al., 2014; Olofsson et al., 2014; Sepich et al., 2011; Shimada et al., 2006). Inhibiting microtubule polymerization disrupts convergent extension, which is known to be regulated by the PCP pathway (Lane and Keller, 1997). In addition, previous work has shown that noncentrosomal apical microtubules are reoriented in response to tissue strain in *Xenopus* ectodermal tissue (Chien et al., 2015). Therefore, we hypothesized that tension might reorient microtubules and bias the trafficking of core PCP components to establish planar polarity. To test this hypothesis, we

Development (2022) 149, dev200515. doi:10.1242/dev.200515

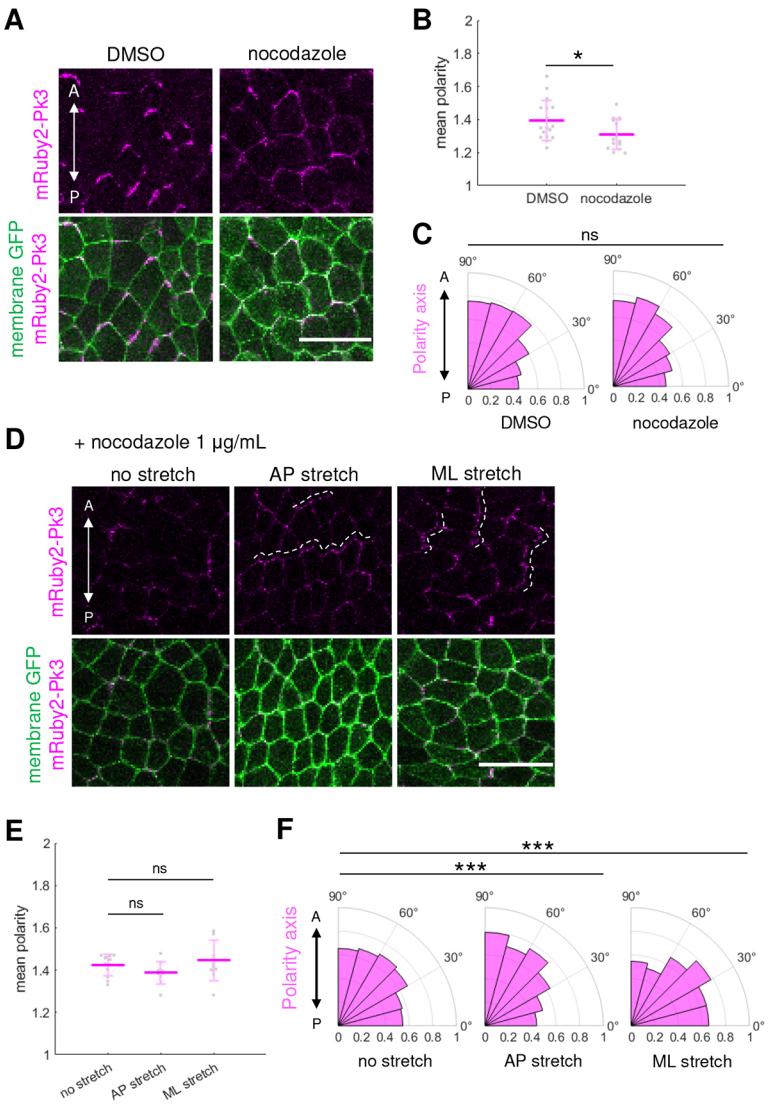

Fig. 6. The determination of the polarity axis by tissue stretch is not microtubule mediated. (A) Fluorescence images of embryos treated with DMSO or nocodazole (1 µg/ml) at stage 14. (B) Plots of the mean polarity. Data are mean±s.d. (C) Plots of the polarity axis. (D) Fluorescence images of explants stretched in 1 µg/ml nocodazole. Dotted line indicates cell-cell interface where mRuby2-Prickle3 accumulated. (E) Plots of the mean polarity. Data are mean±s.d. (F) Plots of the polarity axis. *n*=17 (DMSO) and *n*=15 (nocodazole) embryos in A-C. *n*=12 (no stretch), *n*=10 (AP stretch) and *n*=11 (ML stretch) explants in D-F. The data were obtained from 3 (A-C) or 3 (D-F) independent experiments. Scale bars: 50 µm. In rose plots, the area of each bin represents the relative number of observations. Statistical significance was tested using a two-tailed Mann–Whitney *U*-test in B,E and a Kuiper test in C,F. **P*<0.05, ****P*<0.001. See also Fig. S6.

treated embryos with the microtubule polymerization inhibitor nocodazole during PCP establishment (stages 12-14). We verified that nocodazole treatment significantly perturbed microtubule polymerization (Fig. S6A). Despite this, mRuby2-Prickle3 still showed strong localization at the anterior side of the cells in the presence of nocodazole, although it also weakly localised to other regions of the membranes (Fig. 6A). The mean polarity value decreased due to this more heterogeneous distribution (Fig. 6B). However, the distribution of the polarity axis orientations was not significantly affected by nocodazole treatment (Fig. 6C). These results suggest that directional protein trafficking based on microtubules does not have a significant role in determining the polarity axis but rather acts to strengthen the polarity instructed by other mechanisms.

We further confirmed that microtubules did not play a role during polarity axis establishment in response to stretch. Explants were treated with nocodazole during the whole stretching procedure (stage 12-14) and imaged at stage 14. The accumulation site of mRuby2-Prickle3 in explants treated with nocodazole changed according to the direction of stretch (Fig. 6D), as in untreated explants (Fig. 3). The polarity value was not significantly different between the unstretched and stretched explants (Fig. 6E), and the distribution of the polarity axis was biased towards the AP axis in AP-stretched explants and towards the ML axis in ML-stretched explants (Fig. 6F). These results suggest that the tension-induced polarity axis regulation is not mediated by microtubules.

Cell shape change orients the polarity axis

Next, we considered the possibility that the tension-induced change in cell shape might act as a cue for PCP. When a tissue is stretched uniaxially, the cells also elongate in the same direction. Therefore, we hypothesized that cells may be sensitive to asymmetries in their shape when establishing planar polarity. To investigate this, we measured the angle θ between the cellular major axis and the polarity axis for each cell in normal embryos (Fig. 7A,B). θ showed a distribution biased toward 0° in stages 12 to 14, especially at stage 13 (Fig. 7B). It means that the cellular major axis and the polarity axis tend to coincide during these stages. We further classified the cells of stages 12 to 14 embryos depending on their aspect ratio, and examined their θ distributions. Cells with an aspect ratio smaller than the median of the distribution were classified as rounded cells, and those with an aspect ratio larger than the median were classified as elongated cells. θ showed a distribution closer to 0° in elongated cells than in rounded cells, and this tendency was the same regardless of the direction of the major axis (Fig. 7C, Fig. S7A,B).

Development (2022) 149, dev200515. doi:10.1242/dev.200515

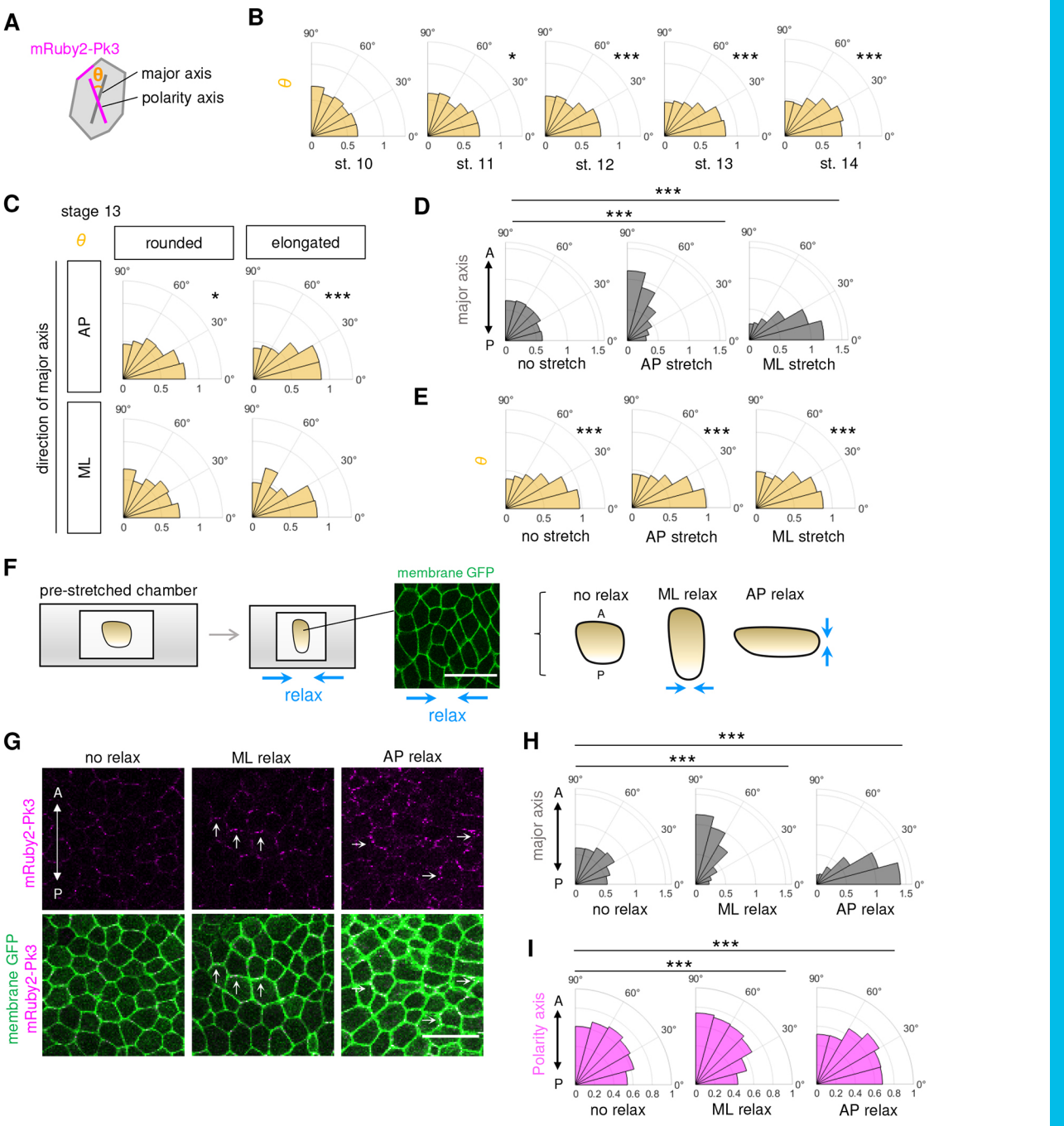

Fig. 7. Cell shape change orients the polarity axis. (A) Schematic image showing the angle θ formed by the major axis and the polarity axis. (B) Plots of θ for stages 10 to 14. (C) Plots of θ for stage 13 sorted by cell shape. A cell was sorted as rounded when its aspect ratio was smaller than the median of the distribution (=1.51). (D,E) Plots of the major axis (D) and θ (E) for explants in stretching experiments. (F) Schematic image showing how to induce cell shape change by relaxing a pre-stretched chamber. (G) Fluorescence images of relaxed explants. Arrows indicate the accumulation of Ruby2-Prickle3. (H,I) Plots of the major axis (H) and the polarity axis (I). n=13 (stage 10), n=15 (stage 11), n=13 (stage 12), n=11 (stage 13) and n=11 (stage 14) embryos in B,C. n=11 (no stretch), n=15 (AP stretch) and n=12 (ML stretch) explants in D,E. n=9 (no relax), n=9 (ML relax) and n=9 (AP relax) explants in G-I. The data were obtained from 3 (B,C), 3 (D,E) or 2 (G-I) independent experiments. In rose plots, the area of each bin represents the relative number of observations. Asterisks in B, C and E indicate a significant difference from uniform distribution. Statistical significance was tested using a Kuiper test. Scale bars: 50 µm. *P<0.05, ***P<0.001. See also Fig. S7.

The same tendency was also observed in embryos treated with blebbistatin and nocodazole, which showed an AP-oriented distribution of the polarity axis as wild-type embryos (Figs S5E,F, S6B,C). These results show that the direction of the cellular major axis and the polarity axis tend to coincide in well-elongated cells when establishing PCP, suggesting that cell elongation contributes to determining the polarity axis.

We further examined θ distributions in uniaxially stretched explants. At the end of the stretching procedure, the cellular major axis was well aligned in the stretch direction in both AP- and ML-stretched explants, while they showed a scattered distribution in unstretched explants (Fig. 7D). As for θ, it showed distributions biased toward 0° in both stretched and unstretched explants (Fig. 7E). These results indicate that, when an explant is

Development (2022) 149, dev200515. doi:10.1242/dev.200515

stretched, cells elongate in the same direction, and that the polarity axis also turns into that direction. Furthermore, the fact that θ distributed close to 0° even in unstretched explants, which showed a scattered distribution of major axis orientations, indicates that the major axis and the polarity axis coincide at the single cell level and it may occur through a cell-autonomous process. When cells were classified depending on their aspect ratio, as in embryos, θ again showed a distribution closer to 0° in elongated cells rather than rounded cells, and this was also the case in unstretched explants (Fig. S7C). These results suggest that cell elongation regulates the direction of the polarity axis, aligning it with the cellular major axis, and that the global alignment of the cellular major axis allows the tissue to obtain a coordinated alignment of the polarity axis.

We conducted another experiment to further confirm the importance of cell shape change in controlling PCP. A neuroectodermal explant was placed on a pre-stretched chamber and then relaxed during the PCP establishment stage to induce cell shape change (Fig. 7F). At the end of the relaxation, the cellular major axis was aligned orthogonally to the relaxation axis (Fig. 7H). mRuby2-Prickle3 accumulated at the AP interfaces of the cells in ML-relaxed explants, whereas it accumulated at the ML interfaces in AP-relaxed explants (Fig. 7G). The polarity axis was oriented in the AP direction in ML-relaxed explants, and in the ML direction in AP-relaxed explants, following the direction of the cellular major axis (Fig. 7I). The mean polarity value showed no significant difference again (Fig. S7D). These results show that the polarity axis was oriented in the same direction as the cellular major axis, even when no exogenous tension was applied, indicating that cell shape change rather than tension plays a significant role in regulating the axis of the planar polarity.

DISCUSSION

The existence of mechanical signalling as a long-range determinant of PCP has been reported in the past decade (Aigouy et al., 2010; Chien et al., 2015, 2018; Ossipova et al., 2015), and, in this study, we showed how mechanical forces affect cell polarity. In addition, our results suggest a cooperative relationship between the mechanical signal and the Wnt signalling. Cells in the posterior neuroectoderm elongate in the AP direction due to a unidirectional tension, which is thought to originate from morphogenetic movements. Our results indicate that cell elongation functions to align cell polarity. The correspondence between the cellular major axis and the polarity axis, and the tendency for the two to be better aligned in well elongated cells, were most pronounced around stage 13, when PCP is first noticeable. In explant stretching experiments, the cellular major axis oriented along the direction of stretch and the polarity axis also aligned in this direction across the whole tissue, even when the orientation of stretch differed from that occurring naturally in embryos along the AP direction. These facts indicate that cell elongation plays a significant role in determining the polarity axis during PCP establishment, although the maintenance of PCP was not investigated in this study. Importantly, although the tissue stretch controlled the orientation of the polarity axis, it did not change the mean polarity value significantly in any of the explant stretching experiments. As the localization of mRuby2-Prickle3 on cell membrane was drastically decreased in tissue ablation experiments (Fig. 2F, Fig. S2C) and Crescent overexpression experiments (Fig. S4A), it is suggested that both tissue integrity along the AP axis and Wnt signalling are required for membrane localization of Prickle and the primary formation of cell polarity.

There are several possible mechanisms through which cell shape change could affect the distribution of the core PCP proteins. One possibility is via rearrangement of tricellular junctions. Both in our results and in previously published immunostaining results (Ossipova et al., 2015), some of the core PCP proteins were particularly concentrated at tricellular junctions. In a tightly packed planar monolayer of cells, the orientation of the cell shape, defined by tricellular junctions, aligns exactly with the principal axis of local stress (Nestor-Bergmann et al., 2018, 2019). Considering these facts, core PCP proteins that accumulate at tricellular junctions by some mechanism might further concentrate to the most anterior tricellular junction via rearrangement in response to tissue stretch. Another possible mechanism is via cell-cell junction transition. When a tissue is stretched, cell shape change is accompanied by anisotropic changes in the junctional area, i.e. the junctions aligned with the direction of stretch elongate and those perpendicular to the direction of stretch shrink. Some of the core PCP proteins show increased stability at shrinking junctions (Butler and Wallingford, 2018), suggesting that junction transitions accompanying cell shape change might promote the accumulation of core PCP proteins at the anterior-posterior interfaces of cells.

In this study, we focused on a mechanical signal as a global cue for PCP and revealed that cell elongation derived from unidirectional tension contributes to determining the polarity axis. However, this cell elongation cannot determine the 'direction' of polarity. In other words, cell elongation would be able to control whether core PCP proteins accumulate to the AP or ML interface of the cells, but not whether they accumulate on the anterior or the posterior side within each cell. Therefore, we think that cell elongation does not work alone but cooperates with other mechanisms to establish PCP *in vivo*. We focused on Wnt signalling as another mechanism and obtained some results suggesting that tissue stretch acts together with the Wnt signalling to regulate planar polarity. In both explants with endogenous Wnts and explants with an ectopic Wnt source, cell polarity did not align uniformly across the tissue in the absence of stretch but showed a high degree of alignment when stretch was applied in the same direction as diffusion of Wnt ligands. When stretch was applied in a direction perpendicular to the Wnt diffusion, polarity was formed in an intermediate direction between the directions of the two PCP regulators. When the endogenous Wnt signalling was partially inhibited by Crescent overexpression, polarity in the ML-stretched explants did not change significantly. These results suggest that tissue stretch alone is not sufficient to induce PCP and that it acts to further regulate the polarity that is primarily induced by the Wnt signalling. In normal development, the directions of tissue stretch and Wnt diffusion are oriented in the AP direction so that they can robustly establish clear planar polarity. Whether mechanical signalling and Wnt signalling interact in this context and how they interact with each other remains to be elucidated.

MATERIALS AND METHODS

Xenopus laevis maintenance and embryo collection

Xenopus laevis were purchased from Watanabe *Xenopus* – inbred strain resource centre (Japan) and kept at 22°C. For embryo collection, female frogs were injected with 300 units of gonadotropin (Kyoritsu Seiyaku, Japan) and kept at 20°C overnight. Testes were dissected from male frogs and kept in DeBoer's solution [110 mM NaCl, 1.3 mM KCl, 0.45 mM $CaCl_2$, 3 mM HEPES and 0.01% kanamycin (pH 7.2)] at 4°C. For fertilization, part of the testis was cut and suspended in DeBoer's solution.

Plasmid construction, *in vitro* transcription and micro injection

Xpk3 CDS was obtained by PCR (template: pXT7moo2-GFP-Xpk3) and subcloned into pCSf107-mRuby2-mT to make pCSf107-mRuby2-Xpk3. The primer sequences used are as follows: forward primer,

Development (2022) 149, dev200515. doi:10.1242/dev.200515

cgggatccCGAGCTCAAGCTTCGAATTC; reverse primer, gctctagattaTG-AAAGAAGGCAACTTTTGT.

mRNAs were synthesized with mMESSAGE mMACHINE SP6 (Thermo Fisher Scientific) according to manufacturer's protocol. For micro-injection, embryos were placed in 5% polysucrose 400 (Wako)/Steinberg's solution [58 mM NaCl, 0.67 mM KCl, 0.34 mM $Ca(NO_3)_2$, 0.83 mM $MgSO_4$, 3 mM HEPES and 0.01% Kanamycin (pH 7.4)]. For injection needle, GD-1 Glass Capillary with Filament (Narishige) was used. mRNAs to detect cell polarity were injected with the following amount per embryo that does not cause any developmental defect to the injected embryos: 150 pg *mRuby2-xPrickle3*, 65 pg *Vangl2*, 100 pg *membrane-tethered GFP*. When injecting *Crescent* mRNA, it was mixed with these mRNAs before injection. *Wnt11* mRNA was injected into an animal ventral blastomere of 32-cell embryo by 300 pg per embryo. Alexa Fluor 647 (Thermo Fisher Scientific) was injected into one side of the embryo to identify the midline. After incubation in 5% polysucrose/Steinberg's solution for 0.5-1 h, medium was changed to 0.1×Steinberg's solution.

Confocal microscopy

Fluorescence images were captured using Nikon Eclipse TiE-VBGR T-C2 (Nikon) with 20× objective. When imaging embryos, a 35 mm glass base dish (IWAKI) was used. Embryos were embedded in 1.2% UltraPure L.M.P Agarose (Thermo Fisher Scientific)/0.1×Steinberg's solution. For explant imaging, they were detached from the stretching chamber with a tungsten needle after fixation and mounted on a slide glass with 50% Glycerol/PBS. *Z* projection images were obtained using Fiji (Schindelin et al., 2012).

Cell polarity measurement

Binarized membrane mask images were obtained from membrane GFP images using Packing Analyser (Aigouy et al., 2010) and used for cell polarity quantification. Cell polarity was quantified using a previously published MATLAB script (Strutt et al., 2016). In brief, fluorescence intensity of polarity protein on the cell membrane was placed into 360 bins depending on their angular orientation from the centre of the cell. After choosing a reference angle, the cell was then subdivided into four quadrants of 90° each. The fluorescence intensity of mRuby2-Prickle3 was summed within each quadrant and diametrically opposed quadrants were added up (e.g. bins in 0-90° and 180-270°). Diametrically opposed quadrants defined two perpendicular axes and the total intensity of fluorescence along each of these axes was compared giving an intensity ratio. This process was repeated with varying the reference orientation in steps of 1°. The angle that gave the maximum intensity ratio was defined as the angle of the polarity axis for that cell, and the corresponding intensity ratio was defined as the mean polarity value of that cell. The mean polarity value is an indicator of how unevenly polarity protein was localized on cell membrane.

To identify individual cells and link polarity information with cell shape information, the mean polarity, the polarity axis and the coordinate of the centroid of the cell were extracted for each cell. The angle of the polarity axis was expressed as 90° for the anterior-posterior axis of the embryo. When analysing cell polarity by PCA method, Quantify Polarity, a software package published by Tan et al. (2021), was used.

Cell shape analysis

The same membrane mask images as Polarity Measurement were used to analyse cell shape. To calculate the aspect ratio and the major axis angle, cells were first approximated as ellipses using the regionprops function in MATLAB. Aspect ratio was defined as the length of the major axis compared with that of the minor axis. The angle of the major axis was expressed as 90° for the anterior-posterior axis of the embryo. Cell shape information was linked to cell polarity information cell by cell, by referencing the coordinates of the centroid of the cell. The angle formed by the major axis and the polarity axis was calculated for each cell on Microsoft Excel. Cells were grouped as 'rounded' or 'elongated' based on their aspect ratio: a cell was grouped as a rounded cell when its aspect ratio was smaller than the median in that experiment, and the rest of the cells were grouped as elongated cells. The direction of the major axis of the cell was grouped as ML when it was in the range of 0°-45°, and as AP when it was in the range of 45°-90°.

Laser ablation

Laser ablation experiments were conducted on a Nikon Eclipse TiE-VBGR T-C2. Embryos were placed under the same conditions as described in the 'Confocal microscopy' section. A 100% 405 nm laser pulse was irradiated for 30 s in a straight line over the region of three to five cells. Embryos underwent laser ablation at stage 12 and were incubated until stage 14. The relaxed area was defined as the area from the ablation site to about 10 cells away along the axis perpendicular to the ablation line (shadowed areas in Fig. 2D,H, Fig. S2A,E). The area estimated not to experience much effect of relaxation in the same embryo was used as the control area so that we could obtain an internal control for each sample. The ablation site was 5-10 cells away from the blastopore in experiments in Fig. 2D-K, and 15-20 cells away from the blastopore in Fig. S2A-H.

Hemi-section

Embryos underwent laser ablation were fixed with MEMFA (0.1 M MOPS, 2 mM EGTA, 1 mM $MgSO_4$ and 3.7% formaldehyde) for 2 h at room temperature and incubated in 1×sucrose solution (0.2×PBS, 0.3 M sucrose and 0.05% Tween 20) for 10 min. A half of the solution was discarded and an equal volume of 4% LMP Agarose (Thermo Fisher Scientific)/1×sucrose solution was added (the final concentration of LMP Agarose was 2%). All the solution and embryos were replaced on a 35 mm dish (IWAKI) and placed at 4°C until the gel was fully hardened. Embryos were cut with a razor in a direction perpendicular to the ablation line and fixed again in MEMFA for 30 min.

Immunostaining

Embryos were fixed with MEMFA for 1.5-2 h at room temperature then incubated in distilled water for 10 min to remove vitelline membrane. After dehydration, they were incubated in 100% ethanol at −20°C for at least one night. The rehydrated embryos were washed with TBT [50 mM Tris, 150 mM NaCl and 0.1% Triton X-100 (pH 7.4)] and incubated in blocking solution. Blocking was carried out in 10% BSA/TBT for 2 h at room temperature for microtubule staining and in 10% FBS/TBT for 2 h at 4°C for Vangl2 staining. For Vangl2 staining, embryos were incubated in 1% Antigen Unmasking Solution (Vector Laboratories) for 20 min at 95°C before blocking. After blocking treatment, primary antibody was added and embryos were incubated overnight at 4°C. After washing the embryos with TBT, secondary antibody was added and the embryos were incubated overnight at 4°C. Observation was carried out immediately after washing again with TBT. The antibodies and their concentrations used were as follows: 1/200 anti-ZO-1 (61-7300, lot 1087989A, Invitrogen), 1/200 anti-ZO-1 (33-9100, lot UG286808, Invitrogen), 1/500 anti-alpha-tubulin (T9026, batch 0000089497, Sigma-Aldrich), anti-Vangl2 (HPA027043, lot B101376, Sigma-Aldrich), 1/500 anti-mouse IgG Alexa 488 (A-11029, lot 2277759, Invitrogen) and 1/500 anti-rabbit IgG Alexa 594 (A11012, lot 1933366, Invitrogen).

InFor phalloidin staining, fixed embryos were incubated in 100× diluted Alexa Fluor 488 Phalloidin (Invitrogen) in PBS for 20 min at room temperature After washing with PBS, they were imaged using a confocal microscope.

Explant stretching/relaxing

The posterior neuroectoderm was dissected from stage 10.5 embryo in 1×Steinberg's solution. The explant was immediately placed on a stretch chamber STB-CH-04 (Strex) coated with fibronectin. The surface of the explant was gently pushed with the tungsten needle soon after placing to make it flat. Explants were then incubated at 26°C until the reference embryos reached stage 12. The chamber, which had a starting width of 20 mm, was stretched by 2 mm every 25 min using STB-100-4 (Strex). The stretch was repeated five times so that the width of the chamber reached 30 mm at the end of the experiment. It was confirmed that the reference embryos reached stage 14 at the end of each experiment. After stretch, explants were fixed with MEMFA for 2 h at room temperature and washed with PBS. For control samples (unstretched samples), explants were dissected, incubated using the same procedure and left static.

Development (2022) 149, dev200515. doi:10.1242/dev.200515

In the relaxing experiment, an explant was placed on a pre-stretched chamber with a width of 30 mm and incubated until the reference embryos reached stage 12. The chamber was then relaxed by 2 mm every 25 min.

Chemical treatment

To examine the effect of myosin activity inhibition on PCP establishment, embryos were treated with 100 µM blebbistatin (Sigma)/0.1×Steinberg's solution from stage 12 to 14 at 20°C and washed with 0.1×Steinberg's solution. For control samples, the same volume of DMSO was used.

To examine the effect of inhibition of microtubule polymerization on PCP establishment, embryos were treated with 0.001% nocodazole (Cayman Chemical)/0.1×Steinberg's solution from stages 12 to 14 at 20°C and washed with 0.1×Steinberg's solution. For control samples, the same volume of DMSO was used. In explant stretching experiments, the reagent was added to the medium immediately before the first stretch.

Atomic force microscopy

Elasticity was measured using a JPK Nanowizard CellHesion 200 (Bruker) equipped with an *x*-*y* motorized stage and mounted on an inverted fluorescence microscope (IX71, Olympus). A 15 µm diameter polystyrene microsphere (Thermo Fisher Scientific) was attached to a tipless nitride cantilever MLCT-O10 (Bruker) with UV curing glue LOCTITE AA 350 (Henkel). The spring constant of cantilevers was calculated using the thermal noise method, and cantilevers with a spring constant between 0.03 and 0.06 N/m were used for both embryos and explants. Force-distance curves were acquired under the following conditions; setpoint: 3-5 nN, extend speed: 5 µm/s, sample rate: 1024 Hz. All AFM data were analysed with the JPK Data Processing software (JPK). The apparent elasticity was calculated based on the Hertz/Sneddon model for an indentation depth of 2 µm, which is small compared with the cell height (Harris and Charras, 2011).

When measuring the elasticity of embryos, vitelline membranes were removed, and the embryos were placed on a dish covered with modelling clay with an embryo-sized indentation to maintain the sample in place. Measurements were conducted in 0.1×MMR [10 mM NaCl, 0.2 mM KCl, 0.1 mM $MgSO_4$, 0.2 mM $CaCl_2$, 0.5 mM HEPES, 0.01 mM EDTA (pH 7.4)]. During measurements, an area 400 µm×100 µm aligned with the embryo AP axis was mapped in two blocks of 200 µm×100 µm areas, because of the large changes in *z* height occurring along the AP axis. Acquisition of each area took about 20 min. The order in which each block of force maps was acquired was changed randomly. Force-distance curves were acquired at a spatial interval of 12.5 µm in *x* and *y*.

When measuring the elasticity of explants, a stretch chamber was set up upon a *x*-*y* motorized stage. Measurements were conducted in 1×Steinberg's solution. The measurement area was 400 µm×50 µm and force-distance curves were acquired at a spatial interval of 12.5 µm in *x* and *y*.

Quantification and statistical analysis

All statistical tests in this study were performed using MATLAB (MathWorks). Statistical significance of difference between two experimental groups in the mean polarity, the wound width and the apical cell area was tested using a two-tailed Mann–Whitney *U*-test for all experiments except laser ablation experiments. For laser ablation experiments, the significance was tested by two-tailed Wilcoxon signed rank test, because the internal control was acquired for each sample. In rose plots, the area of each bin represents the relative number of observations. Whether the distribution of the major axis, the polarity axis and θ formed by these two axes are significantly different from uniform distribution was tested using a Kuiper test (a circular analogue of the Kolmogorov–Smirnov test) with a previously published code (Berens, 2009). In beeswarm plots, each dot represents the mean value in each embryo or explant. Differences were considered statistically significant when $P<0.05$, and significance is indicated by asterisks in the figures as $*P<0.05$, $**P<0.01$, $***P<0.001$ and $****P<0.0001$. The exact value of *n* and what *n* represents are described in figure legends.

Acknowledgements

We thank Dr Roberto Mayor for sharing *Xenopus* embryos, Dr Sergei Y. Sokol for gifting pXT7moo2-GFP-Xpk3 and Dr Yusuke Miyanari for gifting mRuby2 CDS.

Competing interests

The authors declare no competing or financial interests.

Author contributions

Conceptualization: S.H., T.M.; Methodology: S.H., Y.M., G.C., T.M.; Formal analysis: S.H.; Investigation: S.H.; Resources: Y.M., G.C., T.M.; Data curation: S.H., T.M.; Writing - original draft: S.H.; Writing - review & editing: Y.M., G.C., T.M.; Supervision: T.M.; Project administration: T.M.; Funding acquisition: S.H., Y.M., G.C., T.M.

Funding

This work was supported by the Japan Society for the Promotion of Science (JSPS) (19J22652 to S.H., 18K06244, 18H04967, 19H04948 and 21K06183 to T.M., and 18K14720 to Y.M.), the Japan Science and Technology Agency (JPMJPR194B to Y.M.) and the European Research Council (ERC; MolCellTissMech, agreement 647186 to G.C.). S.H. is a research fellow of the JSPS and was a research fellow of JSPS Overseas Challenge Program for Young Researchers in collaboration with the ERC.

Peer review history

The peer review history is available online at https://journals.biologists.com/dev/article-lookup/doi/10.1242/dev.200515.

References

Aigouy, B., Farhadifar, R., Staple, D. B., Sagner, A., Röper, J.-C., Jülicher, F. and Eaton, S. (2010). Cell flow reorients the axis of planar polarity in the wing epithelium of Drosophila. *Cell* **142**, 773-786. doi:10.1016/j.cell.2010.07.042

Aw, W. Y., Heck, B. W., Joyce, B. and Devenport, D. (2016). Transient tissue-scale deformation coordinates alignment of planar cell polarity junctions in the mammalian skin. *Curr. Biol.* **26**, 2090-2100. doi:10.1016/j.cub.2016.06.030

Axelrod, J. D. (2013). Mathematical modeling of planar cell polarity signaling. *Springer Proc. Math.* **15**, 27-35. doi:10.1007/978-3-642-20164-6_4

Berens, P. (2009). CircStat: a MATLAB toolbox for circular statistics. *J. Stat. Softw.* **31**, 108291. doi:10.18637/jss.v031.i10

Butler, M. T. and Wallingford, J. B. (2017). Planar cell polarity in development and disease. *Nat. Rev. Mol. Cell Biol.* **18**, 375-388. doi:10.1038/nrm.2017.11

Butler, M. T. and Wallingford, J. B. (2018). Spatial and temporal analysis of PCP protein dynamics during neural tube closure. *Elife* **7**, e36456. doi:10.7554/eLife.36456

Carron, C., Bourdelas, A., Li, H.-Y., Boucaut, J.-C. and Shi, D.-L. (2005). Antagonistic interaction between IGF and Wnt/JNK signaling in convergent extension in Xenopus embryo. *Mech. Dev.* **122**, 1234-1247. doi:10.1016/J.MOD.2005.06.007

Chen, W. S., Antic, D., Matis, M., Logan, C. Y., Povelones, M., Anderson, G. A., Nusse, R. and Axelrod, J. D. (2008). Asymmetric homotypic interactions of the atypical cadherin flamingo mediate intercellular polarity signaling. *Cell* **133**, 1093-1105. doi:10.1016/j.cell.2008.04.048

Chien, Y.-H., Keller, R., Kintner, C. and Shook, D. R. (2015). Mechanical strain determines the axis of planar polarity in ciliated epithelia. *Curr. Biol.* **25**, 2774-2784. doi:10.1016/j.cub.2015.09.015

Chien, Y.-H., Srinivasan, S., Keller, R. and Kintner, C. (2018). Mechanical strain determines cilia length, motility and planar position in the left-right organizer. *Dev. Cell* **45**, 316-330.e4. doi:10.1016/j.devcel.2018.04.007

Chu, C.-W. and Sokol, S. Y. (2016). Wnt proteins can direct planar cell polarity in vertebrate ectoderm. *eLife* **5**, e16463. doi:10.7554/eLife.16463

Devenport, D. (2014). The cell biology of planar cell polarity. *J. Cell Biol.* **207**, 171-179. doi:10.1083/jcb.201408039

Ewen-Campen, B., Comyn, T., Vogt, E. and Perrimon, N. (2020). No evidence that Wnt ligands are required for planar cell polarity in Drosophila. *Cell Rep.* **32**, 108121. doi:10.1016/j.celrep.2020.108121

Gao, B., Song, H., Bishop, K., Elliot, G., Garrett, L., English, M. A., Andre, P., Robinson, J., Sood, R., Minami, Y. et al. (2011). Wnt signaling gradients establish planar cell polarity by inducing Vangl2 phosphorylation through Ror2. *Dev. Cell* **20**, 163-176. doi:10.1016/j.devcel.2011.01.001

Goodrich, L. V. and Strutt, D. (2011). Principles of planar polarity in animal development. *Development* **138**, 1877-1892. doi:10.1242/dev.054080

Gray, R. S., Roszko, I. and Solnica-Krezel, L. (2011). Planar cell polarity: coordinating morphogenetic cell Behaviors with embryonic polarity. *Dev. Cell* **21**, 120-133. doi:10.1016/j.devcel.2011.06.011

Hannus, M., Feiguin, F., Heisenberg, C. P. and Eaton, S. (2002). Planar cell polarization requires widerborst, a B' regulatory subunit of protein phosphatase 2A. *Development* **129**, 3493-3503. doi:10.1242/dev.129.14.3493

Harris, A. R. and Charras, G. T. (2011). Experimental validation of atomic force microscopy-based cell elasticity measurements. *Nanotechnology* **22**, 345102. doi:10.1088/0957-4484/22/34/345102

Jenny, A. (2010). Planar cell polarity signaling in the drosophila eye. *Curr. Top. Dev. Biol.* **93**, 189-227. doi:10.1016/B978-0-12-385044-7.00007-2

Jenny, A., Darken, R. S., Wilson, P. A. and Mlodzik, M. (2003). Prickle and strabismus form a functional complex to generate a correct axis during planar cell polarity signaling. *EMBO J.* **22**, 4409-4420. doi:10.1093/emboj/cdg424

Ku, M. and Melton, D. A. (1993). Xwnt-11: a maternally expressed Xenopus wnt gene. *Development* **119**, 1161-1173. doi:10.1242/dev.119.4.1161

Lane, M. C. and Keller, R. (1997). Microtubule disruption reveals that Spemann's organizer is subdivided into two domains by the vegetal alignment zone. *Development* **124**, 895-906. doi:10.1242/DEV.124.4.895

Luxenburg, C., Heller, E., Pasolli, H. A., Chai, S., Nikolova, M., Stokes, N. and Fuchs, E. (2015). Wdr1-mediated cell shape dynamics and cortical tension are essential for epidermal planar cell polarity. *Nat. Cell Biol.* **17**, 592-604. doi:10.1038/ncb3146

Mahaffey, J. P., Grego-Bessa, J., Liem, K. F. and Anderson, K. V. (2013). Cofilin and Vangl2 cooperate in the initiation of planar cell polarity in the mouse embryo. *Development* **140**, 1262-1271. doi:10.1242/dev.085316

Matis, M., Russler-Germain, D. A., Hu, Q., Tomlin, C. J. and Axelrod, J. D. (2014). Microtubules provide directional information for core PCP function. *Elife* **3**, e02893. doi:10.7554/eLife.02893

Nestor-Bergmann, A., Goddard, G., Woolner, S. and Jensen, O. E. (2018). Relating cell shape and mechanical stress in a spatially disordered epithelium using a vertex-based model. *Math. Med. Biol.* **35**, i1-i27. doi:10.1093/imammb/dqx008

Nestor-Bergmann, A., Stooke-Vaughan, G. A., Goddard, G. K., Starborg, T., Jensen, O. E. and Woolner, S. (2019). Decoupling the roles of cell shape and mechanical stress in orienting and cueing epithelial mitosis. *Cell Rep.* **26**, 2088-2100.e4. doi:10.1016/j.celrep.2019.01.102

Olofsson, J., Sharp, K. A., Matis, M., Cho, B. and Axelrod, J. D. (2014). Prickle/spiny-legs isoforms control the polarity of the apical microtubule network in planar cell polarity. *Development* **141**, 2866-2874. doi:10.1242/DEV.105932

Ossipova, O., Kim, K. and Sokol, S. Y. (2015). Planar polarization of Vangl2 in the vertebrate neural plate is controlled by Wnt and Myosin II signaling. *Biol. Open* **4**, 722-730. doi:10.1242/bio.201511676

Peng, Y. and Axelrod, J. D. (2012). Chapter two - asymmetric protein localization in planar cell polarity: mechanisms, puzzles, and challenges. *Curr. Top. Dev. Biol.* **101**, 33-53. doi:10.1016/B978-0-12-394592-1.00002-8

Qian, D., Jones, C., Rzadzinska, A., Mark, S., Zhang, X., Steel, K. P., Dai, X. and Chen, P. (2007). Wnt5a functions in planar cell polarity regulation in mice. *Dev. Biol.* **306**, 121-133. doi:10.1016/j.ydbio.2007.03.011

Schindelin, J., Arganda-Carreras, I., Frise, E., Kaynig, V., Longair, M., Pietzsch, T., Preibisch, S., Rueden, C., Saalfeld, S., Schmid, B. et al. (2012). Fiji: an open-source platform for biological-image analysis. *Nat. Methods* **9**, 676-682. doi:10.1038/nmeth.2019

Sepich, D. S., Usmani, M., Pawlicki, S. and Solnica-Krezel, L. (2011). Wnt/PCP signaling controls intracellular position of MTOCs during gastrulation convergence and extension movements. *Development* **138**, 543-552. doi:10.1242/dev.053959

Shibata, M., Itoh, M., Hikasa, H., Taira, S. and Taira, M. (2005). Role of crescent in convergent extension movements by modulating Wnt signaling in early Xenopus embryogenesis. *Mech. Dev.* **122**, 1322-1339. doi:10.1016/j.mod.2005.06.002

Shimada, Y., Yonemura, S., Ohkura, H., Strutt, D. and Uemura, T. (2006). Polarized transport of Frizzled along the planar microtubule arrays in Drosophila wing epithelium. *Dev. Cell* **10**, 209-222. doi:10.1016/j.devcel.2005.11.016

Shindo, A., Yamamoto, T. S. and Ueno, N. (2008). Coordination of cell polarity during Xenopus gastrulation. *PLoS One* **3**, e1600. doi:10.1371/JOURNAL.PONE.0001600

Singh, J. and Mlodzik, M. (2012). Planar cell polarity signaling: coordination of cellular orientation across tissues. *Wiley Interdiscip. Rev. Dev. Biol.* **1**, 479-499. doi:10.1002/wdev.32

Sokol, S. Y. (2015). Spatial and temporal aspects of Wnt signaling and planar cell polarity during vertebrate embryonic development. *Semin. Cell Dev. Biol.* **42**, 78-85. doi:10.1016/j.semcdb.2015.05.002

Strutt, H., Gamage, J. and Strutt, D. (2016). Robust asymmetric localization of planar polarity proteins is associated with organization into signalosome-like domains of variable stoichiometry. *Cell Rep.* **17**, 2660-2671. doi:10.1016/j.celrep.2016.11.021

Sunyer, R., Conte, V., Escribano, J., Elosegui-Artola, A., Labernadie, A., Valon, L., Navajas, D., García-Aznar, J. M., Muñoz, J. J., Roca-Cusachs, P. et al. (2016). Collective cell durotaxis emerges from long-range intercellular force transmission. *Science* **353**, 1157-1161. doi:10.1126/science.aaf7119.

Tan, S. E., Tan, W., Fisher, K. and Strutt, D. (2021). QuantifyPolarity, a new tool-kit for measuring planar polarized protein distributions and cell properties in developing tissues. *Development*. **148**, dev198952. doi:10.1242/DEV.198952

Tree, D. R. P., Shulman, J. M., Rousset, R., Scott, M. P., Gubb, D. and Axelrod, J. D. (2002). Prickle mediates feedback amplification to generate asymmetric planar cell polarity signaling. *Cell* **109**, 371-381. doi:10.1016/S0092-8674(02)00715-8

Vladar, E. K., Bayly, R. D., Sangoram, A. M., Scott, M. P. and Axelrod, J. D. (2012). Microtubules enable the planar cell polarity of airway cilia. *Curr. Biol.* **22**, 2203-2212. doi:10.1016/j.cub.2012.09.046

Wallingford, J. B. and Harland, R. M. (2001). Xenopus dishevelled signaling regulates both neural and mesodermal convergent extension: parallel forces elongating the body axis. *Development* **128**, 2581-2592. doi:10.1242/dev.128.13.2581

Wang, Y. and Nathans, J. (2007). Tissue/planar cell polarity in vertebrates: new insights and new questions. *Development* **134**, 647-658. doi:10.1242/dev.02772

Wu, J. and Mlodzik, M. (2008). The frizzled extracellular domain is a ligand for Van Gogh/Stbm during nonautonomous planar cell polarity signaling. *Dev. Cell* **15**, 462-469. doi:10.1016/j.devcel.2008.08.004

Wu, J., Roman, A.-C., Carvajal-Gonzalez, J. M. and Mlodzik, M. (2013). Wg and Wnt4 provide long-range directional input to planar cell polarity orientation in Drosophila. *Nat. Cell Biol.* **15**, 1045-1055. doi:10.1038/ncb2806

Yu, J. J. S., Maugarny-Calès, A., Pelletier, S., Alexandre, C., Bellaiche, Y., Vincent, J. P. and McGough, I. J. (2020). Frizzled-dependent planar cell polarity without secreted Wnt ligands. *Dev. Cell* **54**, 583-592.e5. doi:10.1016/j.devcel.2020.08.004

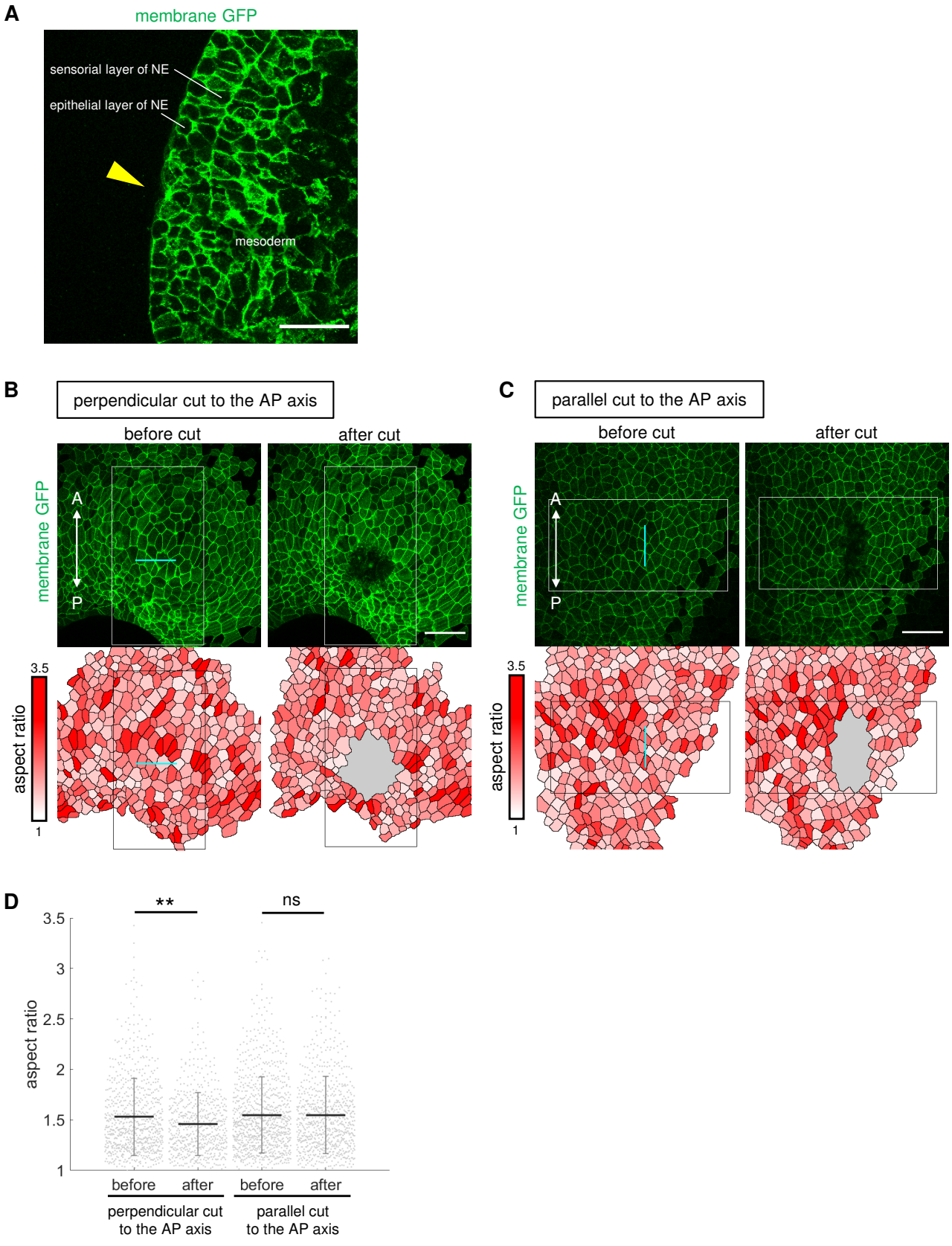

Fig. S1. The effect of laser ablation on tissue and cell morphology (Related to Figure 2)

(A) Cross-sectional view of the embryo ablated perpendicular to the AP body axis. Arrowhead indicates the ablation site. NE, neurectoderm.

(B and C) Images of neuroectodermal tissue ablated perpendicular (B) or parallel (C) to the AP body axis. Lower panels indicate aspect ratio of each cell. Cyan line indicates ablation site. Rectangle indicates anterior/posterior (B) or left/right (C) areas of the cut, which were used for quantifying cell aspect ratio.

(D) Change of cell aspect ratio before/after tissue ablation. Embryo number n= 7 for each condition. The data were obtained from 6 independent experiments. Statistical significance was tested by two-tailed Mann-Whitney U-test.

A, anterior; P, posterior; bp, blastopore. ** = $p < 0.01$. Scale bars, 100 μm.

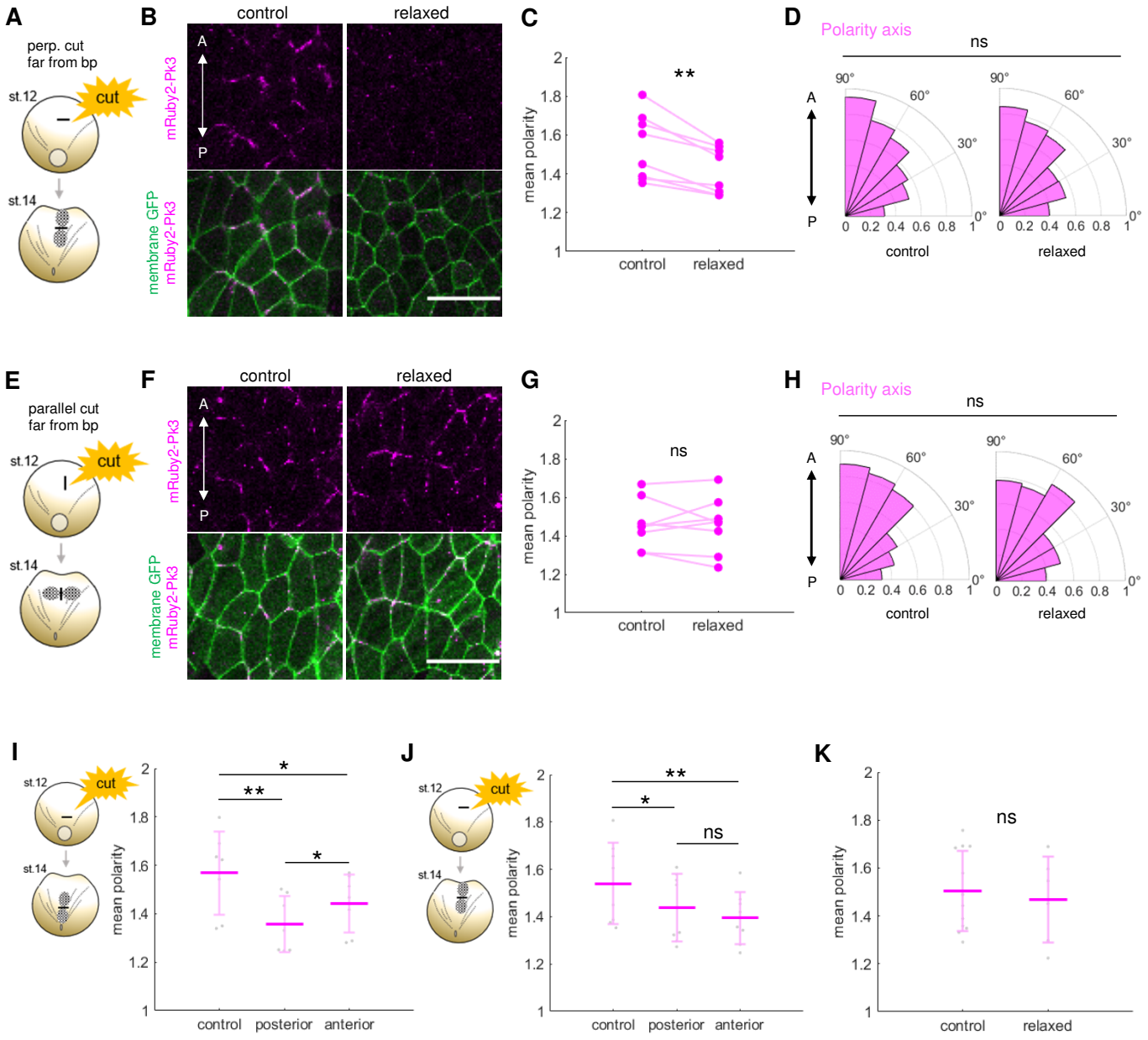

Fig. S2. The effect of laser ablation on polarity formation (Related to Figure 2)

(A and E) Schematic images of laser ablation experiments.

(B and F) Fluorescence images of control and relaxed areas in laser ablation experiments. The 'relaxed' image in (B) shows the posterior side of the cut. Scale bars, 50 μm.

(C and G) Plots of the mean polarity. Lines connect data from the same embryo.

(D and H) Plots of the polarity axis. The area of each bin represents the relative number of observations. Embryo number n = 8 (A-D) and n = 8 (E-H).

(I and J) Plots of the mean polarity when the tissue was cut perpendicular to the AP body axis in a region close to (I) or far from (J) the blastopore. Relaxed region was separated into anterior and posterior regions to the cut. Bars show mean ± s.d.

(K) The mean polarity of the region more than 10 cells away from the cut when the tissue was cut perpendicular to the AP body axis. The data in (I-K) came from the same embryos as in Figures 2D-2G and 2H-2K.

The data were obtained from 4 independent experiments. A, anterior; P, posterior; bp, blastopore. Statistical significance was tested by Wilcoxon signed rank test in (C and G), two-tailed Mann-Whitney U-test in (I-K) and Kuiper test in (D and H). * = $p < 0.05$, ** = $p < 0.01$.

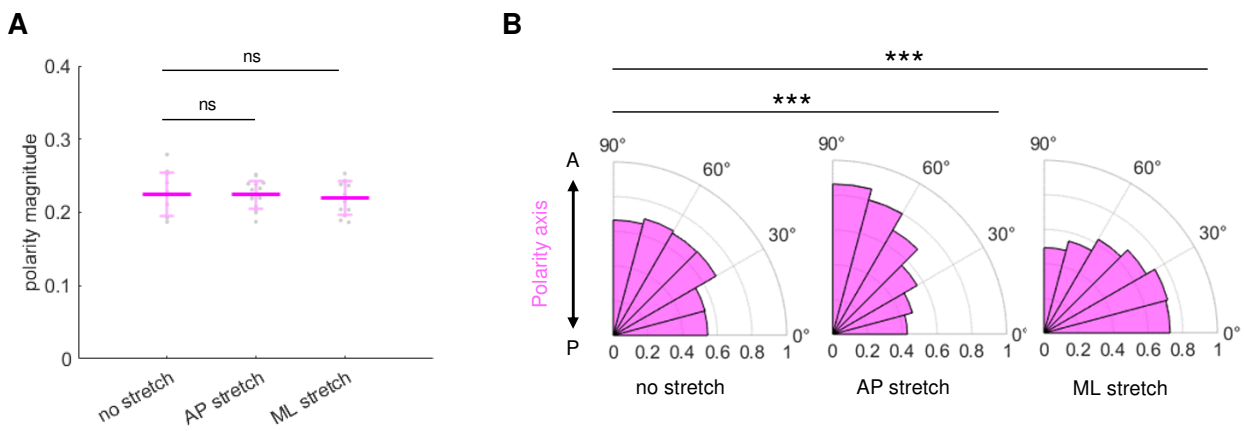

Fig. S3. Polarity analysis by PCA method for the data from explant stretching experiments (Related to Figure 3)

(A) Plots of the polarity magnitude, which corresponds to the mean polarity. Bars show mean ± s.d. **(B)** Plots of the polarity axis. The area of each bin represents the relative number of observations. The same embryos as in Figure 3 were used for the analysis. Statistical significance was tested by two-tailed Mann-Whitney U-test in (A) and by Kuiper test in (B). *** = $p < 0.001$.

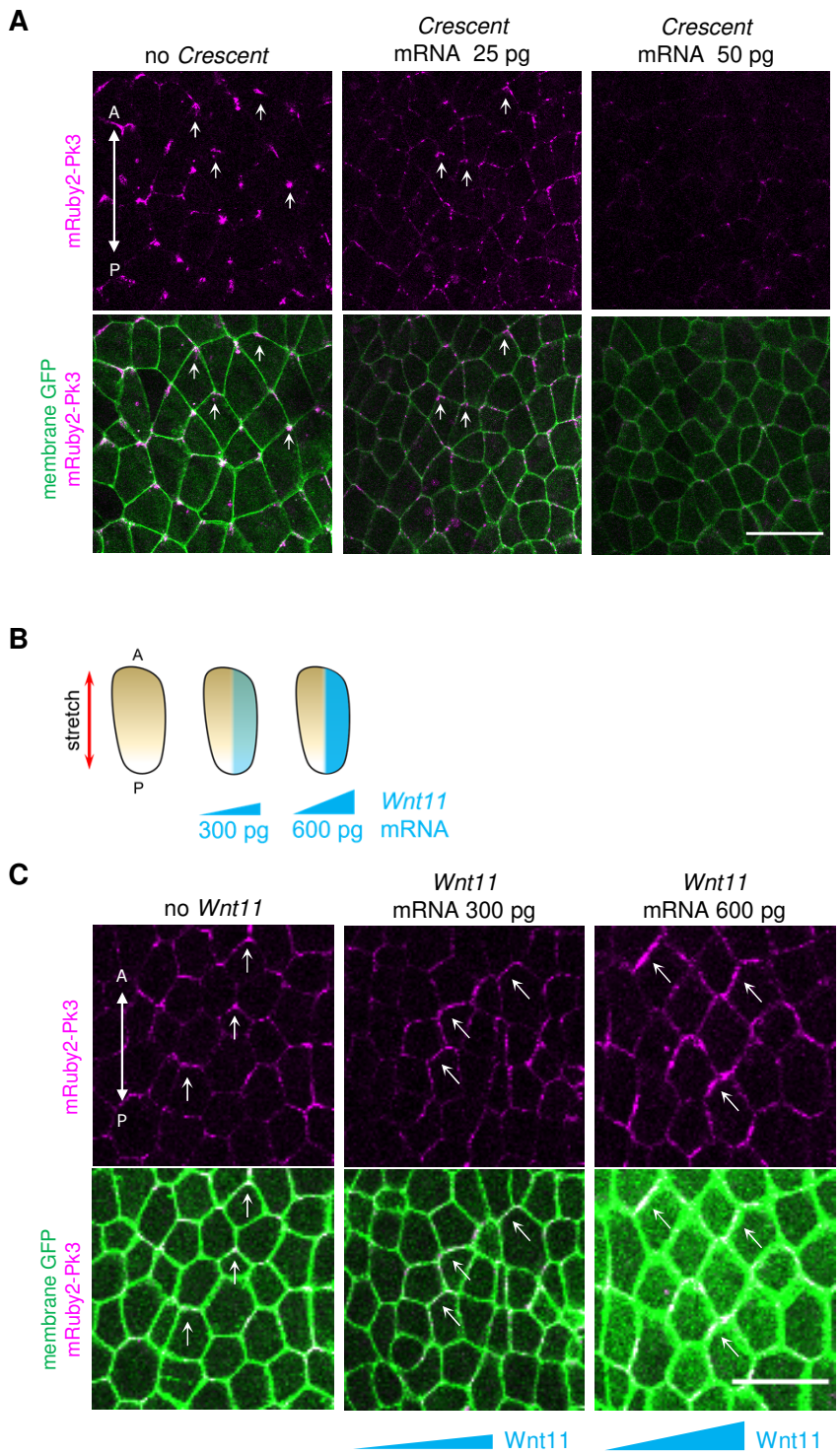

Fig. S4. Crescent or Wnt11 overexpression (Related to Figure 4)

(A) Fluorescence images of embryos overexpressed with Crescent. Arrows indicate the accumulation of mRuby2-Prickle3 at the anterior side of the cell.
(B) Schematic image of stretching experiment. Wnt11 was overexpressed in one side of ventral ectodermal tissue. All the explants were stretched in the AP direction.
(C) Fluorescence images of explants stretched in the method described in (B). Arrows indicate the accumulation of mRuby2-Prickle3. Wnt ligand source is on the right side of the images.
The data were obtained from 2 (A) or 3 (C) independent experiments. A, anterior; P, posterior. Scale bars, 50 µm.

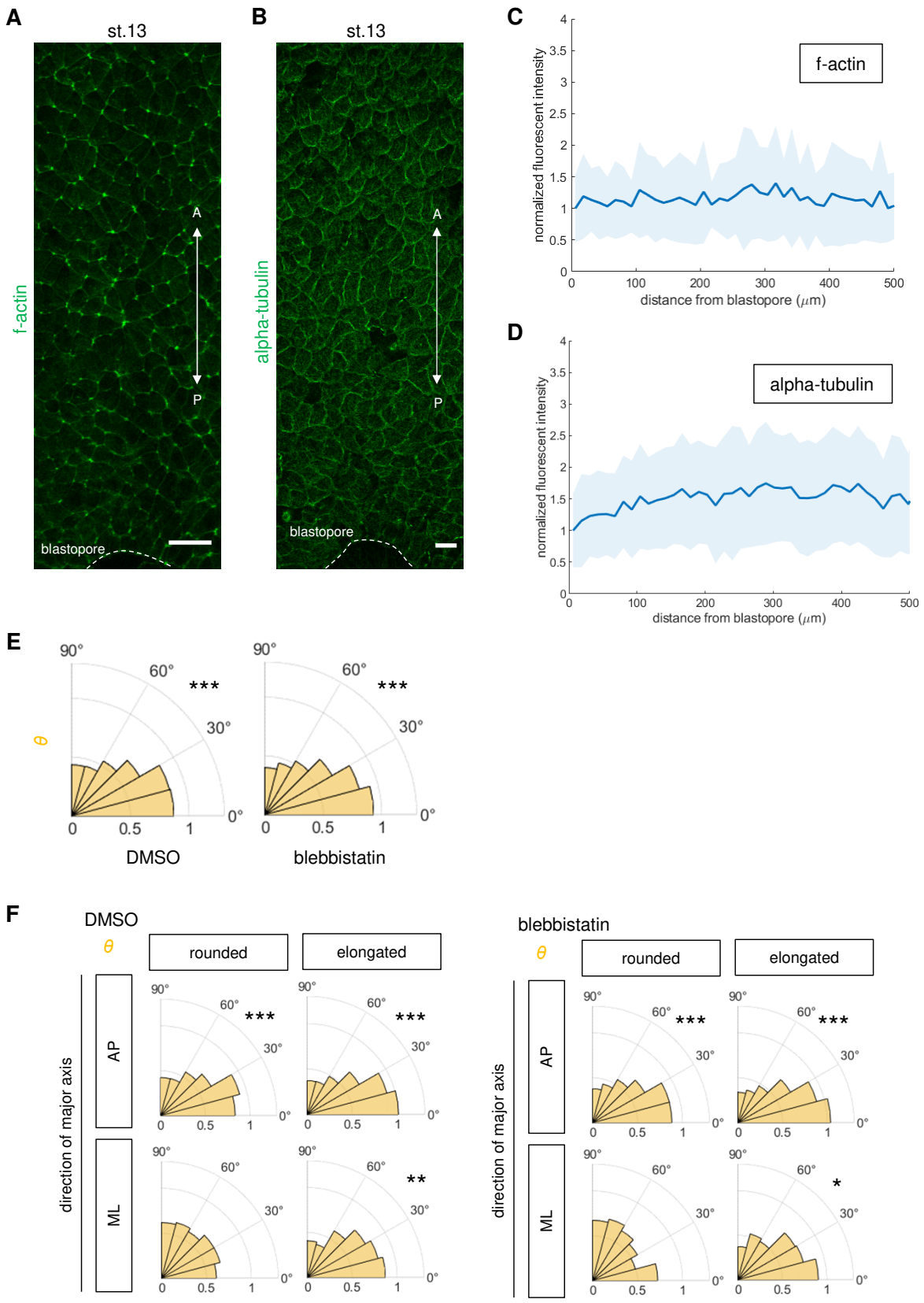

Fig. S5. Cytoskeleton distribution in WT embryos and polarity analysis for blebbistatin-treated embryos (Related to Figure 5)

(A and B) Fluorescence images of stage 13 embryo stained for F-actin (A) or microtubule (B).

(C and D) Plots of fluorescence intensity in (A) or (B) normalized by the average fluorescence intensity of the most posterior region. Line and band show mean ± s.d. The plots are representative of 6 embryos (C) or 9 embryos (D).

(E) Plots of θ (See Figure 7A) for DMSO- or blebbistatin- treated embryos. Asterisks indicate significant difference from uniform distribution. Embryo number n = 11 (DMSO) and n = 12 (blebbistatin).

(F) Plots of θ for DMSO- or blebbistatin-treated embryos sorted by cell shape. A cell was sorted as rounded when its aspect ratio was smaller than the median of the distribution (=1.50 or 1.52 for DMSO or blebbistatin, respectively). Asterisks indicate significant difference from uniform distribution.

The data were obtained from 3 (A, C), 5 (B, D) or 3 (E-F) independent experiments. Statistical significance was tested by Kuiper test in (E and F). * = $p < 0.05$, ** = $p < 0.01$, *** = $p < 0.001$.

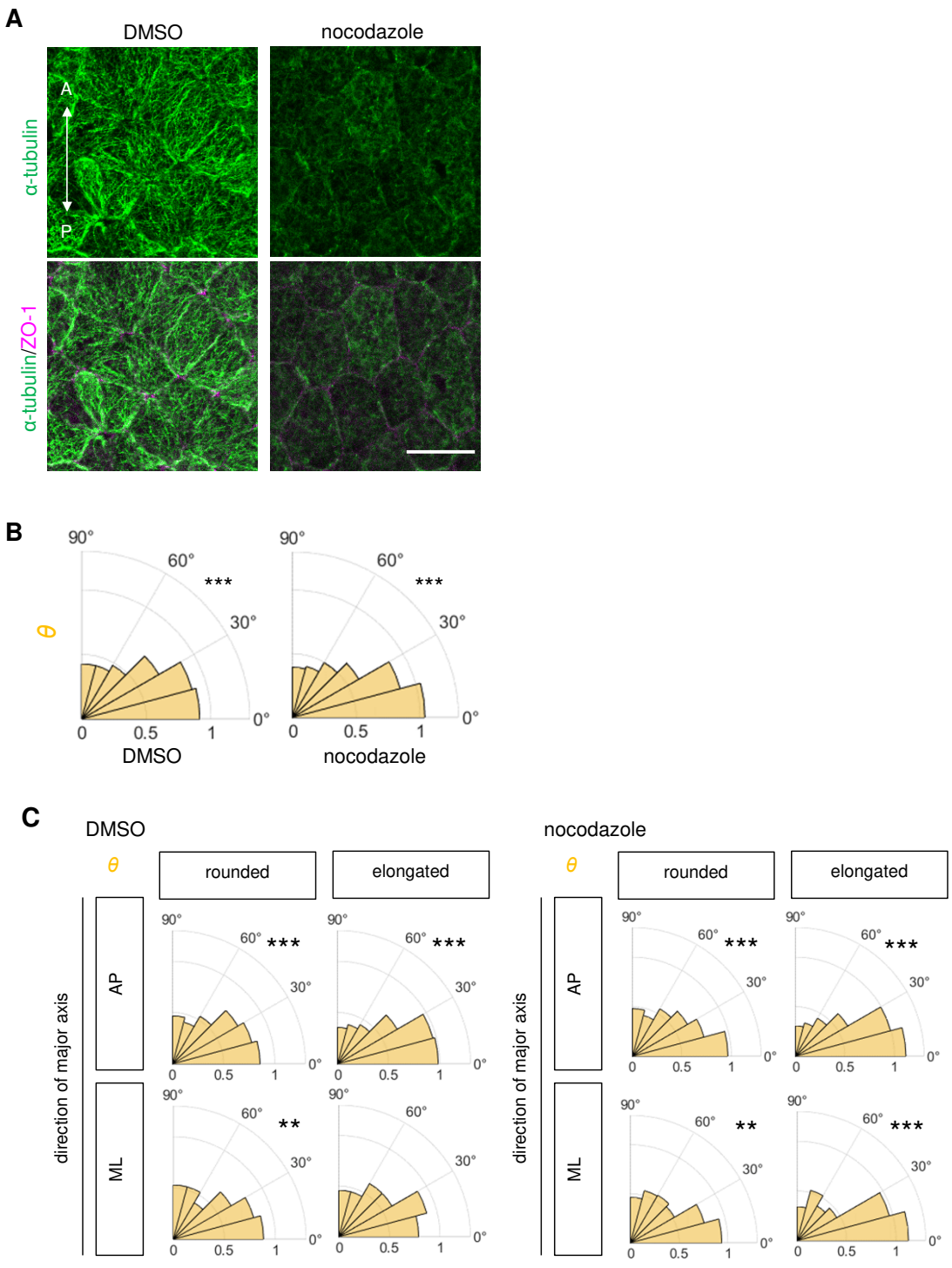

Fig. S6. Nocodazole treatment experiments (Related to Figure 6)

(A) Fluorescence images of immunostained embryos treated with DMSO or nocodazole. Scale bar, 50 μm.
(B) Plots of θ (See Figure 7A) for DMSO- or nocodazole- treated embryos. Embryo number n = 17 (DMSO) and n = 15 (nocodazole).
(C) Plots of θ for DMSO- or nocodazole-treated embryos sorted by cell shape. A cell was sorted as rounded when its aspect ratio was smaller than the median of the distribution (=1.52 or 1.50 for DMSO or nocodazole, respectively).
The data were obtained from 2 (A) or 3 (B-C) independent experiments. Asterisks indicate significant difference from uniform distribution. Statistical significance was tested by Kuiper test. ** = $p < 0.01$, *** = $p < 0.001$.

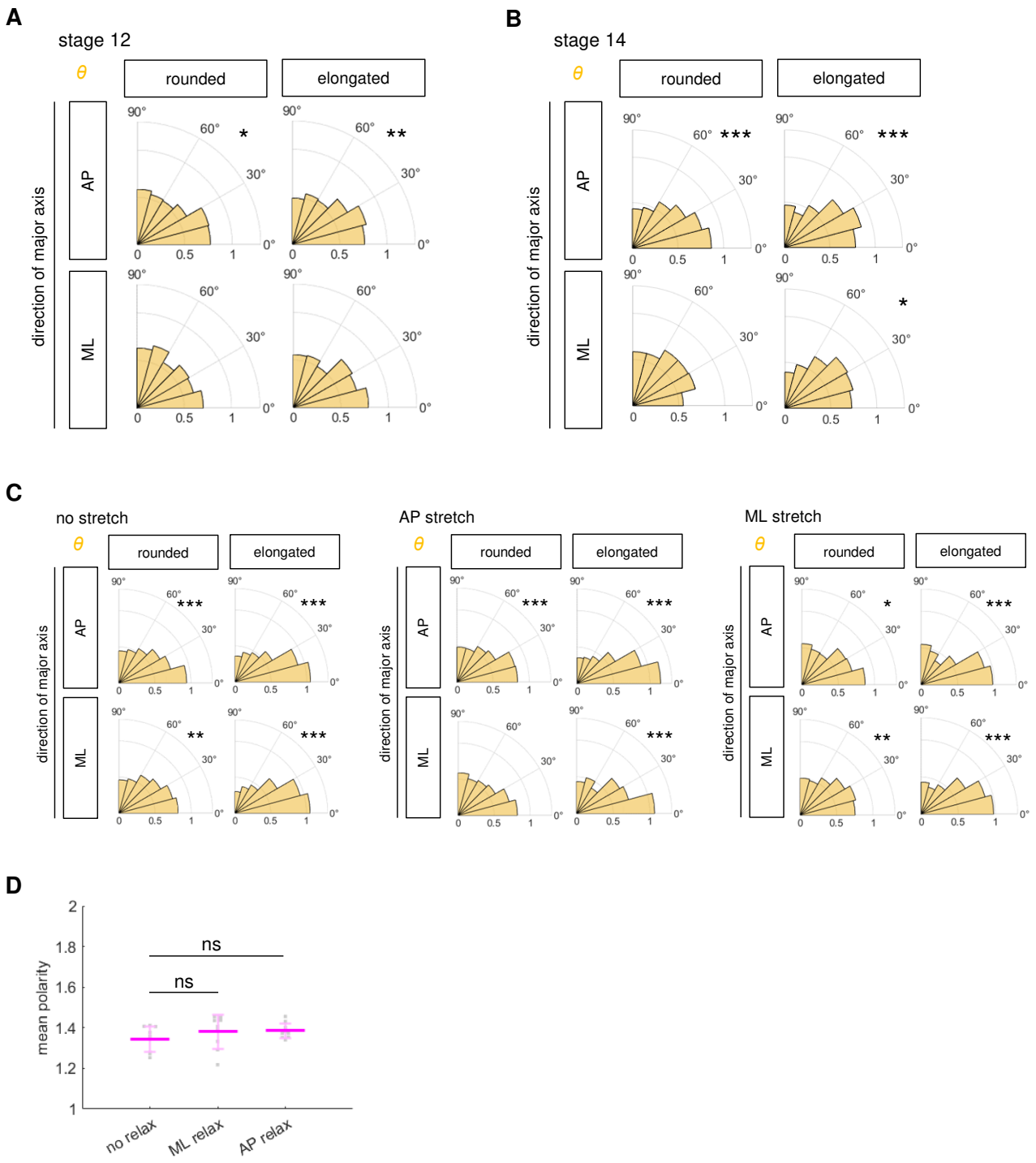

Fig. S7. The coincidence between the major axis and the polarity axis is clearer in elongated cells than in rounded cells (Related to Figure 7)

(A and B) Plots of θ for stage 12 (A) or 14 (B) embryos. Data came from the same embryos as Figure 7B. A cell was sorted as rounded when its aspect ratio was smaller than the median of the distribution (=1.44 or 1.55 for stage 12 or 14, respectively). Embryo number n = 11 (A) and n = 11 (B).

(C) Plots of θ. Data came from the same explants as Figures 7D and 7E. A cell was sorted as rounded when its aspect ratio was smaller than the median of the distribution (=1.29, 1.32 or 1.33 for no, AP or ML stretch, respectively). Explant number n = 11 (no stretch), n = 15 (AP stretch) and n = 12 (ML stretch).

(D) Plots of the mean polarity for explant relaxing experiment (Figure 7F-7I). Bars show mean ± s.d.

The data were obtained from 3 (A-B) 3 (C) or 2 (D) independent experiments. Asterisks indicate significant difference from uniform distribution. Statistical significance was tested by Kuiper test in (A-C) and two-tailed Mann-Whitney U-test in (D). * = $p < 0.05$, ** = $p < 0.01$, *** = $p < 0.001$.